Journal of Controlled Release 353 (2023) 850–863

Contents lists available at ScienceDirect

Journal of Controlled Release

journal homepage: www.elsevier.com/locate/jconrel

Targeted $CuFe_2O_4$ hybrid nanoradiosensitizers for synchronous chemoradiotherapy

Marziyeh Salehiabar [a,b], Mohammadreza Ghaffarlou [c], Ali Mohammadi [a], Navid Mousazadeh [a], Hossein Rahimi [d], Fatemeh Abhari [e], Hamid Rashidzadeh [a], Leila Nasehi [f], Hamed Rezaeejam [e], Murat Barsbay [c], Yavuz Nuri Ertas [g,h], Hamed Nosrati [a,b,**], Taras Kavetskyy [b,i,j,*], Hossein Danafar [a,b,**]

[a] Zanjan Pharmaceutical Biotechnology Research Center, Zanjan University of Medical Sciences, Zanjan, Iran
[b] Joint Ukraine-Azerbaijan International Research and Education Center of Nanobiotechnology and Functional Nanosystems, Drohobych, Ukraine
[c] Hacettepe University, Department of Chemistry, Beytepe, Ankara 06800, Türkiye
[d] Department of Reproductive Biology, Faculty of Advanced Medical Sciences, Tabriz University of Medical Sciences, Tabriz, Iran
[e] Department of Radiology, School of Paramedical Sciences, Zanjan University of Medical Sciences, Zanjan 45139- 56184, Iran
[f] Department of Medical Laboratory, School of Paramedical Sciences, Zanjan University of Medical Sciences, Zanjan, Iran
[g] ERNAM—Nanotechnology Research and Application Center, Erciyes University, Kayseri 38039, Türkiye
[h] Department of Biomedical Engineering, Erciyes University, Kayseri 38039, Türkiye
[i] Department of Materials Engineering, The John Paul II Catholic University of Lublin, 20-950 Lublin, Poland
[j] Drohobych Ivan Franko State Pedagogical University, 82100 Drohobych, Ukraine

ARTICLE INFO

Keywords:
$CuFe_2O_4$
Synchronous
Chemoradiotherapy
Radiosensitizer
Bimetallic nanoparticles

ABSTRACT

Multifunctional nanoplatforms based on novel bimetallic nanoparticles have emerged as effective radiosensitizers owing to their potential capability in cancer cells radiosensitization. Implementation of chemotherapy along with radiotherapy, known as synchronous chemoradiotherapy, can augment the treatment efficacy. Herein, a tumor targeted nanoradiosensitizer with synchronous chemoradiotion properties, termed as $CuFe_2O_4$@BSA-FA-CUR, loaded with curcumin (CUR) and modified by bovine serum albumin (BSA) and folic acid (FA) was developed to enhance tumor accumulation and promote the anti-cancer activity while attenuating adverse effects. Both copper (Cu) and iron (Fe) were utilized in the construction of these submicron scale entities, therefore strong radiosensitization effect is anticipated by implementation of these two metals. The structure–function relationships between constituents of nanomaterials and their function led to the development of nanoscale materials with great radiosensitizing capacity and biosafety. BSA was used to anchor Fe and Cu ions but also to improve colloidal stability, blood circulation time, biocompatibility, and further functionalization. Moreover, to specifically target tumor sites and enhance cellular uptake, FA was conjugated onto the surface of hybrid bimetallic nanoparticles. Finally, CUR as a natural chemotherapeutic agent was encapsulated into the developed bimetallic nanoparticles. With incorporation of all abovementioned stages into one multifunctional nanoplatform, $CuFe_2O_4$@BSA-FA-CUR is produced for synergistic chemoradiotherapy with positive outcomes. *In vitro* investigation revealed that these nanoplatforms bear excellent biosafety, great tumor cell killing ability and radiosensitizing capacity. In addition, high cancer-suppression efficiency was observed through *in vivo* studies. It is worth mentioning that co-use of $CuFe_2O_4$@BSA-FA-CUR nanoplatforms and X-ray radiation led to complete tumor ablation in almost all of the treated mice. No mortality or radiation-induced normal tissue toxicity were observed following administration of $CuFe_2O_4$@BSA-FA-CUR nanoparticles which highlights the biosafety of these submicron scale entities. These results offer powerful evidence for the potential capability of $CuFe_2O_4$@BSA-FA-CUR in radiosensitization of malignant tumors and opens up a new avenue of research in this area.

* Corresponding author at: Joint Ukraine-Azerbaijan International Research and Education Center of Nanobiotechnology and Functional Nanosystems, Drohobych, Ukraine.
** Corresponding authors at: Zanjan Pharmaceutical Biotechnology Research Center, Zanjan University of Medical Sciences, Zanjan, Iran.
E-mail addresses: nosrati.hamed2020@gmail.com (H. Nosrati), kavetskyy@yahoo.com (T. Kavetskyy), danafar@zums.ac.ir (H. Danafar).

https://doi.org/10.1016/j.jconrel.2022.12.004
Received 5 July 2022; Received in revised form 8 November 2022; Accepted 3 December 2022

1. Introduction

The most common methods of cancer treatments include; targeted therapy, chemotherapy, immunotherapy, radiotherapy, systemic therapy, hormone therapy and surgery [1]. Among these modalities, radiation therapy (RT) as an efficient and palliative tool has been applied to >50% of all cancer patients and can extend patient's life expectancy through inducing DNA damage of rapidly proliferating tumor cells [2].

Ionizing radiation can be applied directly to the tumor tissues or employed as a supplementary tool beside other common method of cancer treatments. A growing body of literature has demonstrated that for complete eradication of cancer cells and effectively shrinking them, high doses of radiation are needed and this may increase the risk of damage to neighboring healthy tissues which has always been an unresolved clinical problem and challenge in cancer radiotherapy [3]. Radiotherapy toxicities which account as the major obstacle for radiation dose escalation are namely classified into acute and/or late toxicity [4]. Therefore, curative and effective radiation therapy has faced with the dilemma of how to maximally kill tumor cells while suppressing undesired damage to surrounding healthy tissues. Considerable progress has been made to address these points by developing radiosensitizers and enhancing their potential in cancer radiotherapy [5]. Radiosensitizers make tumor cells more responsive and sensitive to ionizing radiation, consequently facilitating production of free radicals and hastening DNA damages.

The last two decades have seen a rapid progress in development of nanotechnology based materials and by advent of new medical technologies so that promising nanoplatforms with low toxicity to normal tissues can be prepared [6–8]. Nanomaterial-based radiosensitizers have attracted much research interest owing to their excellent physicochemical features, such as intrinsic radiosensitivity, high drug loading capacity, good biocompatibility, and effective tumor-targeting capability by enhanced permeability and retention (EPR) effect [5,9]. These nanoradiosensitizers can also amplify DNA damage through both direct and indirect pathways upon radiation therapy, restrict radioresistance and attenuate radiation damages to normal tissues to accomplish effective radiation-induced cancer therapy with favorable outcomes [10].

Metallic nanoparticles, in particular Fe and Cu based nanomaterials, are competent radiosensitizing agents with capability of augmenting the efficacy of radiotherapy through several mechanisms [11–15]. $CuFeS_2$ [16], Cu_5FeS_4 [17], (BSA)-$CuFeS_2$ [18], Cu_9S_8 [19] and copper-substituted mesoporous silica nanoparticles (Cu-MSNs) [20] have been developed for synergistic tumor therapy. There is also some research that harnessed NPs made of both Fe and Cu elements for cancer therapy [21]. In order to achieve the above purposes and endow potential nanoradiosensitizers, constructing bimetallic nanoplatforms based on Cu and Fe may be an effective strategy in cancer treatment.

In addition to this, the advent of multifunctional nanosystems and advances in developing highly integrated novel bimetallic nanoparticles provide a promising strategy in the fight against cancer [22]. Due to the fact that co-use of modalities will collect the merits of respective individual treatments, the usefulness of multifunctional nanosystems for combined therapy is thus underlined. Combined therapy also offers superior performance to monotherapy in dealing with cancer because it can bring the "$1 + 1 > 2$" effect. In view of that, there has been a shift of focus in clinical research from a single treatment modality to a combined therapy, and it is believed that this will be become a major treatment modality of not only cancer but also other diseases in the near future [23]. Kankala et al. synthesized copper(II)–doxorubicin complexes which conjugated on the surfaces of layered double hydroxide nanoparticles (LDHs) for cancer therapy by the co-delivery system [24].

It is interesting to note that, combination of radiotherapy with other therapeutic modalities would lower dose of radiation energy and can effectively eradicate cancer cells. Accordingly, rational design of multifunctional nanoplatforms along with other innovative approaches to achieve the combination of radiotherapy with other therapeutic modalities is highly needed. However, with all advances in radio oncology, this concern remains an unmet challenge, thus further research is required.

In the current study, to fulfill the above purposes, we developed smart and efficient multifunctional radiosensitizers based on $CuFe_2O_4$ nanoparticles containing curcumin (CUR) to induce a synergistic chemoradiation therapy effect. These nanoparticles were coated with bovine serum albumin (BSA) to improve their blood circulation time, biocompatibility, colloidal stability. Folic acid (FA) was covalently conjugated to nanoparticles in order to tune the surface functionalization and ultimately to improve the targeting specificity. Additionally, due to the presence of both Cu and Fe in construction of these nanoplatforms, great radiosensitivity of tumors is expected through predominant reactive oxygen species (ROS) generation and DNA damage. In other words, $CuFe_2O_4$@BSA-FA nanoplatform not only contributes tumor cells to become more sensitive to ionizing radiation with $CuFe_2O_4$ part, but also exerts a multifunctional therapeutic effect due to the presence of CUR. CUR as a natural bioactive agent has displayed broad range of pharmacological effects, in particular anti-inflammatory and anti-neoplastic activity [25,26]. Beside these, owing to its inherent radiosensitivity, CUR can potentially enhance the efficacy of radiotherapy by arresting tumor cells at the G2/M phase [27]. CUR by down-regulating TNF-inducible NF-κB and AP-1 protein activity induces apoptosis in various carcinomas [28]. Radiation-induced inflammation is another major problem which remains a significant unmet challenge and may cause several complications in radio oncology. Accordingly, anti-inflammatory effects of CUR can ameliorate the aforementioned issue as well as clinical findings highlight that the adverse effects of radiotherapy can be minimized once treatment modality is combined with CUR use [29–31].

Hence, in the current research, we projected a nanoplatform that provides a strong synergistic anticancer effect based on the co-use of CUR and radiation therapy, and all of these can be easily achieved only with using a single innovated nanotherapeutic system. The biosafety and therapeutic potential of the fabricated bimetallic nanoplatform were assessed in detail through both *in vivo* and *in vitro* studies. Fig. 1 depicts the schematic representation of the multi-functional bimetallic nanoplatform used for synchronous chemoradiotherapy.

2. Materials and methods

2.1. Materials

Iron (II) chloride tetrahydrate ($FeCl_2.4H_2O$), copper (II) chloride dehydrate ($CuCl_2{\cdot}2H_2O$), 1-ethyl-3-(3-(dimethylamine)- propyl) carbodiimide (EDC), N-hydroxysuccinimide (NHS), BSA, and curcumin were purchased from Sigma-Aldrich Inc. All other materials and solvents were of analytical grade and were purchased from Merck (Kenilworth, USA) and Sigma- Aldrich (St. Louis, USA) and were used as received with no further purification.

3. Methods

3.1. Synthesis of $CuFe_2O_4$@BSA nanoparticles

The $CuFe_2O_4$@BSA nanoparticles were synthesized through a facile and environmentally friendly strategy. In brief, 50 mL of aqueous solution containing 40 mg $FeCl_2.4H_2O$, 17.00 mg $CuCl_2{\cdot}2H_2O$ and 250 mg BSA was heated to 90 °C. A NaOH solution (2 M, 1.2 mL) was added to adjust the pH of the reaction mixture to ~12. The reaction continued for 30 min at 90 °C, then further continued for 24 h at room temperature. Finally, the resulting product was dialyzed against distilled water for 48 h to obtain the impurity-free $CuFe_2O_4$@BSA nanoparticles. The same protocol was used to synthesize $CuFe_2O_4$ nanoparticles without adding BSA.

3.2. Preparation of folic acid conjugated $CuFe_2O_4$@BSA nanoparticles ($CuFe_2O_4$@BSA-FA)

To bind FA targeting moiety to the albumin portion of bimetallic nanoparticles, the well-known EDC/NHS activation for biochemical conjugations was used. First, the carboxylic acid groups of FA were activated by EDC and NHS and then subjected to nucleophilic attack of amino groups present in BSA molecules. In brief, 42.30 mg EDC and 27.00 mg of NHS along with 20.00 mg FA were mixed in 1.0 mL DMSO. Then, this mixture was gradually added to the aqueous solution containing 200.0 mg of bimetallic $CuFe_2O_4$@BSA nanoparticles. The pH value of the reaction mixture was adjusted to around 8.2 using NaOH solution (1.0 M) and stirred for 24 h. The resulting product was then dialyzed against distilled water for 48 h to obtain the impurity-free $CuFe_2O_4$@BSA-FA nanoparticles.

3.3. Preparation of $CuFe_2O_4$@BSA-FA-CUR hybrid nanoparticles

$CuFe_2O_4$@BSA-FA-CUR hybrid nanoparticles were prepared according to the following procedure: CUR (50.00 mg) was dissolved in DMSO (2.5 mL) and then it was added gradually to the known amount of the pre-synthesized $CuFe_2O_4$@BSA-FA solution. The reaction mixture was stirred at room temperature for 12 h. Finally, the final product was collected by centrifuging at 18000 rpm for 0.5 h and washing several times with deionized water and ethanol (75:25) mixture, followed by a final wash of water, and suspended in phosphate-buffer solution.

3.4. Characterization

Various techniques were used to fully characterize the developed bimetallic hybrid structure. In terms of morphological characterization and size distribution, transmission electron microscopy (TEM, FEI 120 kV) was applied. To characterize the structure of a bimetallic nanoplatform as well as confirm the FA conjugation, FTIR technique (Bruker, Tensor 27, USA) was used. Both hydrodynamic size distribution of developed hybrid system along with their corresponding zeta potential were determined using dynamic light scattering (DLS) on a nano/zetasizer (Malvern Instruments, Worcestershire, UK, ZEN 3600 model Nano ZS). For recording XRD patterns, a powder X-ray diffractometer system (PANalytical X'Pert Powder Diffractometer) was performed. A monochromatized Al Kα X-ray source (Thermo Scientific) was employed for X-Ray photoelectron studies. Energy dispersive spectroscopy (EDS) as a versatile technique that is mostly used to reveal the presence of main elements in the tested materials along with producing elemental distribution maps was used for elemental mapping. In this regard, to confirm the presence of Fe and Cu metals in the developed nanoplatforms, EDS technique was performed. The magnetic property of sample was studied using a vibrating sample magnetometer (VSM).

3.5. Determination of the amount of FA conjugated over $CuFe_2O_4$@BSA

The surface of $CuFe_2O_4$@BSA nanoparticles was modified with FA moieties as targeting ligand through a peptide-like bond (an amide linkage), and UV–vis spectrophotometer (T80 double beam spectrophotometer, PG Instruments Limited) was employed to ascertain the amount of these covalent bonds. In summary, 0.50 mg of $CuFe_2O_4$@BSA-FA and proteinase K enzyme were dispersed in 1.0 mL of PBS:Ethanol mixture (65:35) (pH = 7.4). Afterward, the system was incubated at 37 °C overnight with gentle shaking. Ultimately, after the incubation period, the mixture was centrifuged for 15 min at 18000 rpm

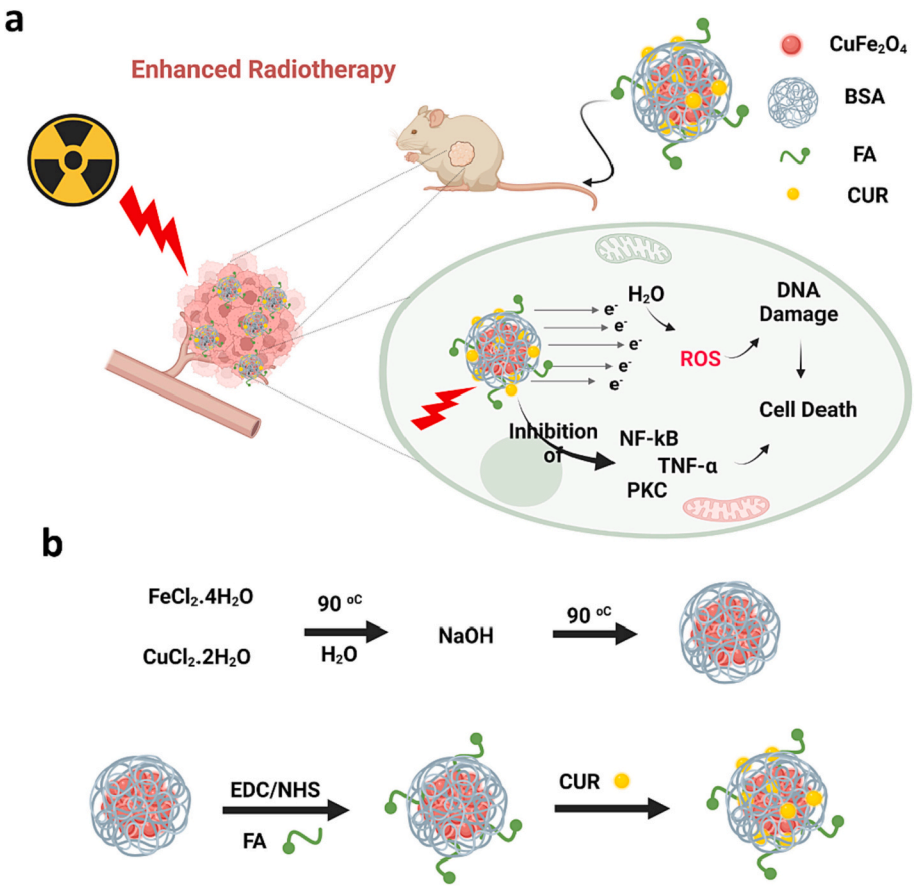

Fig. 1. a) Schematic representation of the multi-functional bimetallic nanoplatform used for synchronous chemoradiotherapy. b) Schematic representation of the synthesis process for preparation of $CuFe_2O_4$@BSA-FA-CUR nanoradiosensitizers.

and subsequently the absorbance of the supernatant containing FA was determined by a UV–vis spectrophotometer at 352 nm.

3.6. CUR loading and release behavior of $CuFe_2O_4$@BSA-FA-CUR

A spectrophotometric investigation at 428 nm was performed to determine the amount of CUR loaded *via* physical adsorption. In brief, known amount of $CuFe_2O_4$@BSA-FA-CUR (3.0 mg) was dispersed in ethanol (1.6 mL), then the prepared dispersion was incubated at 37 °C overnight. After completion of the incubation period, the colloidal dispersion was centrifuged for 15 min at 18000 rpm, and the absorbance of the supernatant containing CUR was determined by a UV–vis spectrophotometer at 428 nm. *In vitro* CUR release profile was studied using dialysis method; accordingly, it was **dialyzed** against PBS:Ethanol (65:35, *v*/v) mixture in both acidic (pH = 4.3) and neutral (pH = 7.4) condition. In brief, known amount of $CuFe_2O_4$@BSA-FA-CUR (0.80 mg) was dispersed in a mixture of PBS:Ethanol (1.0 mL) and transferred into a dialysis bag and then immersed in 35 mL PBS:Ethanol (65:35, v/v). After that, it was incubated at 37 °C with gentle shaking. At the predetermined time intervals, known amount of aliquots were taken from the dialysate and absorbance at 428 nm was measured using a UV–Vis spectrophotometer to disclose the release behavior of CUR from the hybrid bimetallic nanoparticles.

3.7. In vitro assays

3.7.1. Hemocompatibility test

Certain biocompatibility tests considering the toxicity of newly developed nanomaterials should be evaluated prior to reach into the clinical trials. Among them, hemocompatibility of blood-contacting nanomaterials is one of the major criteria for successful clinical application, which can strongly restrict their clinical applicability. Accordingly, the level of hemocompatibility of fabricated bimetallic nanoparticles was performed in accordance with the previously established protocol [32]. In summary, first human erythrocytes were collected and washed with sterile PBS (pH = 7.4). The stock suspension of erythrocytes was prepared and 0.5 mL this suspension was injected to vials containing various treatment groups including $CuFe_2O_4$@BSA-FA, $CuFe_2O_4$@BSA-FA-CUR, PBS (negative control) and deionized water (positive control) with different concentrations (10, 50 and 250 μg/mL). In this step, the prepared nanomaterials come into direct contact with blood cells (red blood cells) and were incubated at 37 °C for 4 h with gentle shaking. After completion of the incubation period, the suspension containing erythrocytes and nanoparticles was centrifuged for 15 min at 15000 rpm, the absorbance of the supernatant containing hemoglobin was determined by a UV–vis spectrophotometer at 540 nm and the hemolysis value was determined using the following equation:

$$\%\text{Hemolysis} = \frac{A\ (sample) - A\ (negative)}{A\ (positive) - A\ (negative)} \times 100$$

Hemolysis assay for each concentration was carried out in triplicates.

3.7.2. Cytotoxicity on HFF-2 cells

In vitro cytotoxicity or MTT assay was carried out to disclose the possible cytotoxic potential of $CuFe_2O_4$@BSA-FA nanoparticles toward healthy cells (HFF-2 cells). It is expected that these nanoparticles would exhibit no cytotoxicity against non-malignant cell line. Therefore, to elucidate this hypothesis, HFF-2 cells were seeded in a 96-well plate (5×10^3 cells per well) and incubated for 24 h. Next, the medium was discarded and new media containing $CuFe_2O_4$@BSA-FA nanoparticles at different concentration (10, 50 and 250 μg/mL) was introduced to each well. After incubation for 5 h, the medium was then removed and replaced with fresh medium and further incubated for 24 h. Afterward, MTT solution (20 μL with concentration of 5 mg/mL) was added to each well. The purple formazan crystals were formed during the incubation period of 4 h, and the media was discard. Subsequently DMSO (100 mL to each well) was added to dissolve these insoluble crystals. Accordingly, the optical density (OD) was read using a microplate reader (Bio-Tek, USA) at 570 nm. This analysis was performed in quintuplicates ($n = 5$).

3.7.3. In vitro anti-cancer activity

Cytotoxicity potential of CUR, $CuFe_2O_4$@BSA-FA and $CuFe_2O_4$@BSA-FA-CUR nanoparticles was evaluated on the mouse breast carcinoma cell line (4T1 cells). This assay was performed to spell out the potential anti-cancer effects of the final nanoformulation. Similarly, MTT test was carried out according to the above mentioned protocols but in the presence and absence of X-ray irradiation. Briefly, after 4T1 cells were seeded and incubated in a 96-well plate (5×10^3 cells per well), then were treated with CUR, $CuFe_2O_4$@BSA-FA and $CuFe_2O_4$@BSA-FA-CUR nanoparticles at different concentrations (5.40, 21.66 and 86.60 44 μg/mL of CUR and the equivalent amount carrier), and free medium was considered as the control group. After 5 h of incubation, the medium containing nanoparticles was removed, and wells were washed with PBS, and fresh medium was then added. Afterward, cells were exposed to X-ray (4 Gy, 6 MV) and then incubated for further 24 h. Finally, MTT assay was used to ascertain the *in vitro* anti-cancer efficacy of developed nanoparticles against 4T1 cells upon X-ray radiation. Of note, MTT assay was also performed without X-ray radiation to evaluate whether the radiotherapy is effective or not in reducing the cell viability of cancer cells.

3.7.4. Cellular uptake and internalization efficacy

$CuFe_2O_4$@BSA and $CuFe_2O_4$@BSA-FA nanoparticles were labeled with fluorescein isothiocyanate (FITC) to evaluate whether the FA ligands are effective in promoting cellular internalization and targeting capability of developed nanoparticles or not. It is expected that FA conjugation would potentially enhance intracellular trafficking of $CuFe_2O_4$@BSA-FA nanoparticles in comparison with non-targeted nanoparticles. In this context, 4 T1 cells were seeded in a 24-well plate at a density of 5×10^4 cells per well. Next, the confluency of cells reached to the desired amount (80%), cells were co-incubated with as prepared FITC-labeled nanoparticlesfor 5 h. Then, cells were washed to remove any impurities such as debris prior to analysis *via* flow cytometer (BD Biosciences, San Jose, CA).

3.7.5. Intracellular ROS generation

It has been well documented that excessive ROS levels can kill tumor cells through activation of various cell death pathways, such as autophagy and apoptosis along with induction of oxidative damages to biomolecules [34]. Therefore, it is expected that ROS-promoting nanomaterials such as $CuFe_2O_4$@BSA-FA-CUR is effective for killing cancer cells by enhancing the curative effect of radiation therapy (X-ray), potentially suppressing tumor growth. To fully elucidate the potential of developed $CuFe_2O_4$@BSA-FA-CUR nanoplatforms in cancer radiotherapy, intracellular ROS generation assay was applied according to the previously reported protocol [35].

3.7.6. Calcein AM/PI cell staining assay

4T1 cells were seeded in a 96well plate (5×10^3 cells per well) and incubated for 24 h, then cells were subjected to various treatments groups including control, X-ray, CUR, CUR + X-ray, $CuFe_2O_4$@BSA-FA, $CuFe_2O_4$@BSA-FA+ X-ray, $CuFe_2O_4$@BSA-FA-CUR and $CuFe_2O_4$@BSA-FA-CUR + X-ray. Afterward, calcein AM (3 μM) which stain viable cells were added to the treated cells and incubated for 30 min. Next, propidium iodide solution (PI, 24 μM) which stains dead cells and incubated for 5 min. Eventually, the green and red fluorescence images were obtained which represented the live and dead 4T1 cells, respectively.

3.7.7. Apoptosis assay

It has been well documented that programmed cell death through a p53-dependent pathway also occurs during radiation therapy [36]. In such condition, programmed cell death is a favor and can be potentiated

by some newly developed and effective nanoplatforms such as $CuFe_2O_4$@BSA-FA-CUR. Therefore, the amount of cell apoptosis caused by CUR, $CuFe_2O_4$@BSA-FA and $CuFe_2O_4$@BSA-FA-CUR in the presence and absence of X-ray radiation was determined according to the previously reported protocol [37].

3.8. Clonogenic assay

This cell biology technique is regarded as an *in vitro* cell survival assay which evaluates the ability of a single cell to grow into a colony. Thus, for assesing the potential radiosensitizing capacity of developed $CuFe_2O_4$@BSA, $CuFe_2O_4$@BSA-FA, $CuFe_2O_4$@BSA-FA-CUR nanoparticles and free CUR in the presence of X-ray irradiation, clonogenic assay was performed according to the previously reported method [38].

3.9. In vivo assays

3.9.1. LD_{50} analysis as an in vivo safety indicator

In vivo safety assessment of developed $CuFe_2O_4$@BSA-FA nanoparticles was investigated using the median lethal dose (LD_{50}). In this test, BALB/c female mice (~20 g weight) as an animal model was used to determine the possible *in vivo* toxicity of synthesized nanoradiosensitizers. Accordingly, $CuFe_2O_4$@BSA-FA at various concentrations ranging from 50 to 400 mg/kg was administrated to the mice by intravenous injection ($n = 4$ mice per dose). To determine the LD_{50}, body weight and survival rate of mice were then monitored for three weeks. Also, blood indexes was analyzed on the first, 14th, and 28th day post-treatment with $CuFe_2O_4$@BSA-FA-CUR.

3.9.2. In vivo antitumor activity

In vivo antitumor activity of CUR, $CuFe_2O_4$@BSA-FA and $CuFe_2O_4$@BSA-FA-CUR nanoparticles was exploited against the mouse breast cancer model in the presence and absence of X-ray radiation. Accordingly, murine breast tumor model was established by subcutaneous injection of about 1×10^6 4T1 cells into the right flank of BALB/c female mice. After about two weeks of inoculation, the tumor volume was determined by means of a digital caliper in two directions of length (L) and width (W) using the following formula: $V = 0.5 \times L \times W^2$. After tumor volumes reached to 80 mm^3, mice were randomized into eight groups of 5 mice. Randomized mice groups were then treated with different regimens as follows: (1) CUR, (2) CUR with 4Gy X-ray, (3) $CuFe_2O_4$@BSA-FA, (4) $CuFe_2O_4$@BSA-FA with 4Gy X-ray, (5) $CuFe_2O_4$@BSA-FA-CUR (6) $CuFe_2O_4$@BSA-FA-CUR with 4Gy X-ray, (7) PBS and (8) X-ray. Of note, all of the aforementioned chemotherapeutics were intravenously injected into the mice through the tail vein. Then, both body weight and tumor volume of each mouse were precisely monitored during the experimental time periods.

For *in vivo* biodistribution study major organs were collected and digested with nitric acid. The accurate contents of Fe were determined by ICP-AES, and then the corresponding distributions of $CuFe_2O_4$@BSA and $CuFe_2O_4$@BSA-FA-CUR were calculated as percentages of injected dose per gram of tissue (%ID/g).

3.9.3. Histopathology analysis

Hematoxylin and eosin (H&E) were used to stain and investigate different organsand tumor histopathology. Typically, on the 16th day of treatment, mice of different groups were euthanized and their major organs such as the kidney, spleen, liver, heart and tumor were collected and fixed in 4% paraformaldehyde, embedded in paraffin and sectioned at 5 mm. These major organs along with tumors were then analyzed with inverted microscopy after being stained with H&E.

3.10. Statistical analysis

All of the quantitative data were expressed as mean with standard deviation (mean ± SD) unless otherwise stated. Statistical analysis was performed using GraphPad Prism software (GraphPad Prism 8).

4. Result and discussion

4.1. Fabrication of $CuFe_2O_4$@BSA-FA-CUR

Biomineralization in nature is the process of producing inorganic biominerals through the regulation of biological macromolecules in living organisms. In the laboratory-scale synthesis of nanocrystals such as $CuFeS_2$ [18], Fe_3O_4 [39], and CuS [40], this nature-inspired process has been adapted as a facile and green synthesis route, where selective interactions with inorganic ions are involved and scaffolds for mineral growths are provided, mostly through functional proteins. BSA, the most abundant protein in blood plasma with numerous active chemical groups such as carboxyl, amino and thiol groups, can interact with various metal ions *via* strong coordination interactions and acts as a biocompatible and water-soluble stabilizing and constitutive guide protein for the production of nanoparticles *via* mimicking biomaterialization processes. In our design, $CuFe_2O_4$@BSA-FA-CUR nanoradiosensitizers were synthesized through three simple steps: (i) Preparation of $CuFe_2O_4$@BSA: BSA was employed as the commercially available and biocompatible template for controlling the growth of $CuFe_2O_4$ nanocrystal. After the addition of NaOH, the alkaline environment promotes BSA to unfold its tertiary configuration and reveal more available functional groups, resulting in a loose structure that triggers crystal growth and encapsulation of nanoparticles [39,40]. It is worth mentioning that BSA plays a fundamental role in this process, not only by anchoring Fe and Cu ions and guiding the crystal-growth, but also by improving the physical stability as well as increasing biocompatibility and functionality of nanoparticles. Zheng et al. previously synthesized citrate-stabilized $CuFe_2O_4$ nano clusters using a simple solvothermal route by the reaction of the same precursor salts (*i.e.* $FeCl_3{\cdot}6H_2O$ and $CuCl_2{\cdot}2H_2O$) in the presence of ethylene glycol and an alkali source [41]. The fact that the method we present here was carried out in a completely aqueous environment and at a lower temperature under the guidance of BSA reveals the advantage of our synthesis method. (ii) Fabrication of $CuFe_2O_4$@BSA-FA: In this step, thanks to the active amine groups of BSA, it was possible to modify with targeting moiety, FA. The carboxylic acid groups of FA activated using EDC and NHS reacted with the amine moieties of BSA in $CuFe_2O_4$@BSA to form amide bonds. (iii) Development of $CuFe_2O_4$@BSA-FA-CUR nanoradiosensitizer: Finalization of the nanoradiosensitizer formulation was accomplished by loading CUR on FA-modified nanoparticles through the phenomenon of physical adsorption to achieve the goal of synchronous chemoradiation therapy. The schematic representation of all these three steps for the preparation of $CuFe_2O_4$@BSA-FA-CUR nanoradiosensitizers is shown in Fig. 1b. UV − Vis spectrophotometry was utilized to determine the amount of FA conjugated to surface of $CuFe_2O_4$@BSA. The amount of conjugated FA was found to be ~8.30 mg per 100 mg of the final formulation. Due to the presence of FA, together with the targeting ability of $CuFe_2O_4$@BSA-FA-CUR, cellular uptake and nanoparticle accumulation are expected to enhance significantly compared to the non-targeted nanoparticles [42–44]. For example, Tonbul et al. recently demonstrated that nano-sized mesoporous silica decorated with FA moieties can kill breast cancer cells at a higher rate compared to the non-targeted mesoporous silica nanoparticles [44].

4.2. Characterization

Several techniques have been applied to characterize the as-prepared nanoplatforms. In terms of size and morphology of the synthesized $CuFe_2O_4$@BSA and $CuFe_2O_4$@BSA-FA-CUR nanoplatforms, TEM was performed (Fig. 2a-c). It was shown that $CuFe_2O_4$ without capping with BSA tends to aggregate (Fig. 1Sa). However, after coating with BSA it was shown better dispersity and stability.

The developed nanoplatforms were monodispersed and spherical in

shape (Fig. 2d-e). AFM image of $CuFe_2O_4$@BSA-FA-CUR indicates a smooth surface with fine particle distribution (Fig. 2f and Figure 1Sb). In order to elucidate the composition and chemical environment of $CuFe_2O_4$@BSA along the surface extending from the top monolayer to a depth of about 10 nm, we carried out XPS analysis. Furthermore, TEM-EDS mapping was applied to investigate the presence and distribution of Cu, Fe and O elements in the final nanoplatform (Fig. 2g), which confirmed the chemical composition of $CuFe_2O_4$@BSA-FA-CUR. In addition, the SEM image and SEM-EDS elemental mappings of $CuFe_2O_4$@BSA-FA-CUR (Fig. 2S) confirmed the presence of Fe, C, N, O and Cu elements in the final formulation of $CuFe_2O_4$@BSA-FA-CUR, which further strengthens our confidence in the successful fabrication of this nanoradiosensitizer. Fig. 2h shows the high-resolution Fe 2p core levels for photoelectrons emitted from $CuFe_2O_4$@BSA, which clearly show the Fe $2p_{3/2}$ peak centered at ~711.1 eV and the Fe $2p_{1/2}$ peak appearing at 724.6 eV. The previously reported binding energies for the Fe $2p_{3/2}$ and Fe $2p_{1/2}$ peaks of copper ferrite ($CuFe_2O_4$) are in excellent agreement with our data [45,46]. It is worth noting that the presence of Fe^{3+} species in the structure causes a satellite peak to appear, usually around 719.2 eV [45,47,48]. The satellite peak in the Fe 2p XPS spectrum at 719.1 eV confirms that the oxidation state of Fe in $CuFe_2O_4$@BSA is Fe^{3+}. High resolution Cu 2p spectrum for $CuFe_2O_4$@BSA is presented in Fig. 2i. The core-level Cu 2p spectrum of $CuFe_2O_4$@BSA is split into two peaks corresponding to Cu $2p_{1/2}$ (953.2 eV) and Cu $2p_{3/2}$ (933.3 eV). The Cu 2p valence state information is in an agreement with previous data [45]. Concerning the Cu 2p spectrum in Fig. 2i, the Cu $2p_{3/2}$ satellite located on the higher binding energy side (~941.5 eV) indicates that the divalent state of copper (Cu^{2+}) is present in the sample [49,50], confirming the chemical environment of Cu in $CuFe_2O_4$.

The zeta potential is a key parameter in stability of a colloidal system. If all suspended particles bear a negative or positive charge, the particles tend to repel each other than to aggregate, colloidal stability is thus enhanced. The tendency of particles to repel each other is directly related to the surface charge or zeta potential value. The surface charge of nanoparticles plays an important role in their circulation in the bloodstream as well as interaction or adhesion with cell layers. The zeta potential of $CuFe_2O_4$@BSA, $CuFe_2O_4$@BSA-FA and $CuFe_2O_4$@BSA-FA-CUR nanoparticles were found to be −15.5, −20 and − 22.3 mV, respectively (Fig. 3a). The mean hydrodynamic sizes of $CuFe_2O_4$@BSA, $CuFe_2O_4$@BSA-FA and $CuFe_2O_4$@BSA-FA-CUR nanoparticles were 31, 52 and 70 nm, respectively, as seen in Fig. 3b. It is worth to mention that the corresponding mean hydrodynamic size increases with the addition of FA and CUR to the $CuFe_2O_4$@BSA nanoparticle formulation. Overall, the negative zeta potential of −22.3 mV along with nanoscale particle size of 70 nm make $CuFe_2O_4$@BSA-FA-CUR an ideal candidate for biological applications, including *in vitro*, *in vivo* and even preclinical studies. Finally, the physical stability in terms of mean hydrodynamic particle size was monitored for 50 days (Fig. S3). No significant particle size changes were detected during the test period, which underlines the excellent colloidal stability of $CuFe_2O_4$@BSA-FA-CUR nanoformulation without aggregation. Of note, the size measured by DLS differs from that obtained by TEM, which can be attributed to the fact that nanoparticles undergo hydration in DLS due to the presence of water, while in TEM the solvent is evaporated. UV–Vis spectrophotometry was also used to confirm the successful synthesis of $CuFe_2O_4$@BSA-FA-CUR. The main absorbance peak of BSA molecules was presented in the spectrum of $CuFe_2O_4$@BSA nanoparticles at 268 nm (Fig. 3c). In addition, two new absorbances of FA molecule were observed at 293 and 334 nm. These results confirm the existence of BSA and FA in the structure of $CuFe_2O_4$@BSA-FA nanoradiosensitizer, verifying the successful synthesis. Furthermore, a broad peak around 400 nm is seen in the UV–Vis spectrum of $CuFe_2O_4$@BSA-FA-CUR, which is attributed to CUR molecules and approves the loading of CUR into the final nanoradiosensitizer formulation. Another commonly used technique for the characterization of nanocrystals is X-ray diffraction (XRD) analysis, which is a simple and fast method that provides useful information regarding the lattice parameters and crystalline grain size, phase and structure [51]. Herein, XRD was applied to investigate the crystalline structure of $CuFe_2O_4$ and $CuFe_2O_4$ @BSA nanoparticles (Fig. 3d). In the XRD pattern of $CuFe_2O_4$@BSA nanoparticles, the broad peak observed at $2\theta = 20^\circ$ indicates the presence of BSA. Comparing the XRD pattern of

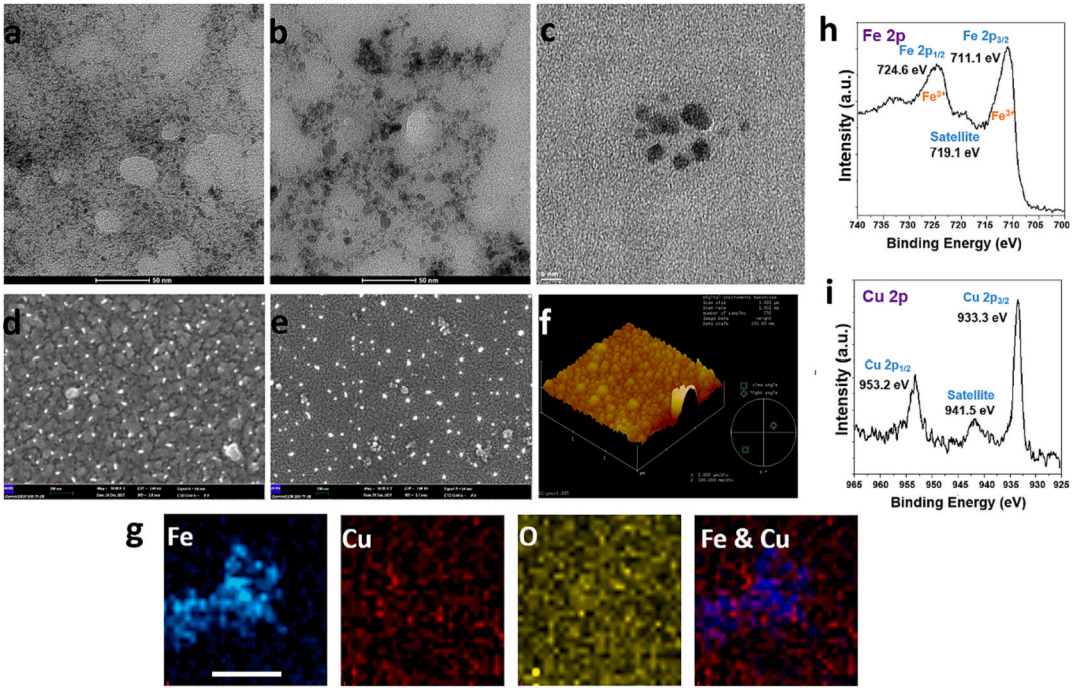

Fig. 2. Morphology and chemical composition analyses of nanoplatforms. (a) TEM images of $CuFe_2O_4$@BSA; (b and c) TEM images of $CuFe_2O_4$@BSA-FA-CUR; FESEM image of (d) $CuFe_2O_4$@BSA and (e) $CuFe_2O_4$@BSA-FA-CUR; (f) AFM image; (g) TEM-EDS mapping analysis of $CuFe_2O_4$@BSA-FA-CUR nanoplatforms (Scale bar = 10 nm); (h) High-resolution X-ray photoelectron Fe 2p spectra of $CuFe_2O_4$@BSA; (i) High-resolution X-ray photoelectron Cu 2p spectra of $CuFe_2O_4$@BSA.

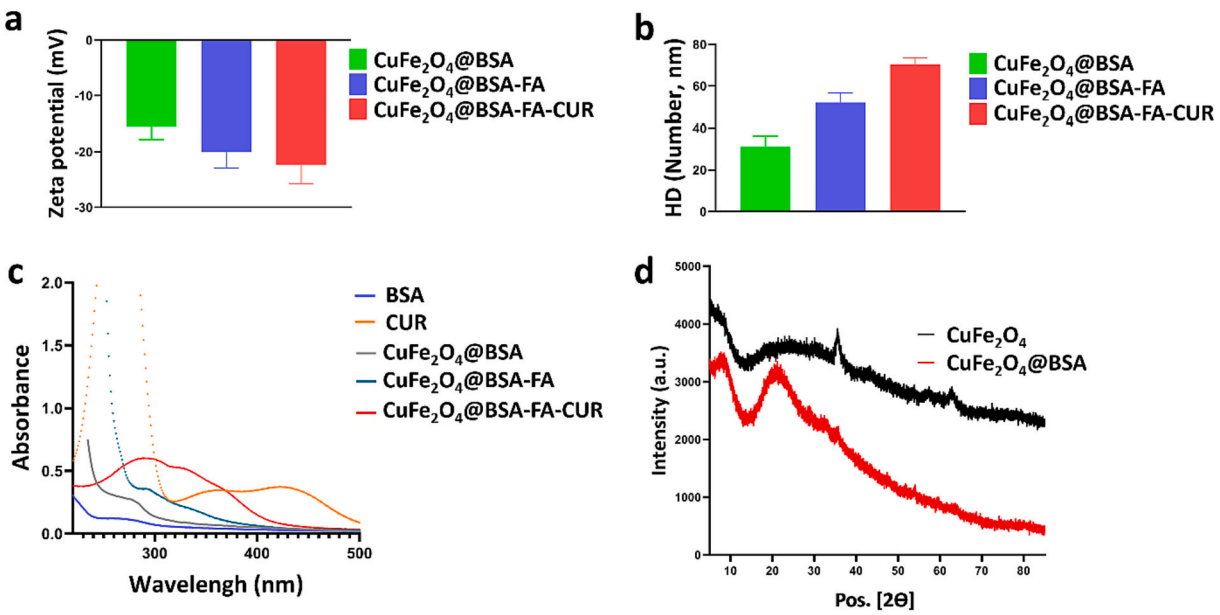

Fig. 3. Characterization. (a) Zeta potentials of nanoparticles; (b) Mean hydrodynamic particles size; (c) UV–Vis spectra of CUR, BSA, $CuFe_2O_4$@BSA, $CuFe_2O_4$@BSA-FA and $CuFe_2O_4$@BSA-FA-CUR and (d) XRD patterns of $CuFe_2O_4$ and $CuFe_2O_4$@BSA nanoparticles.

$CuFe_2O_4$@BSA with the standard XRD card (JCPDS No. 25–0283), the presence of all corresponding $CuFe_2O_4$ peaks was validated [52]. The magnetic property of $CuFe_2O_4$@BSA was studied using a VSM at room temperature, Fig. 4S. The saturation magnetization (M_S) value of the nanoparticles was 1 emu/g. VSM analysis also confirms having of magnetic propertiesin the hybrid system. To verify the bonding FA onto $CuFe_2O_4$@BSA, FTIR technique was applied (Fig. 5S). In the FTIR spectrum of $CuFe_2O_4$@BSA-FA, peaks related to amide I and amide II are seen at the 1639 cm^{-1} and 1518 cm^{-1} regions, respectively, along with another peak indicating the presence of FA at 1738 cm^{-1}. Thus, the conjugation of FA onto the $CuFe_2O_4$@BSA nanoparticles is underlined. Moreover, in the FTIR spectrum of $CuFe_2O_4$@BSA-FA-CUR nanoparticle, in addition to the presence of the characteristic peaks of other components, the main characteristic bands of CUR appear at 530 cm^{-1}, 803 cm^{-1}, 952 cm^{-1}, and 1204 cm^{-1}, which confirms the successful synthesis of the final nanoradiosensitizer formulation.

4.3. CUR loading and release behavior

The *in vitro* drug release of CUR from the as-prepared $CuFe_2O_4$@BSA-FA-CUR nanoradiosensitizers was studied to determine the release profile of CUR under different conditions. Entrapment efficiency and

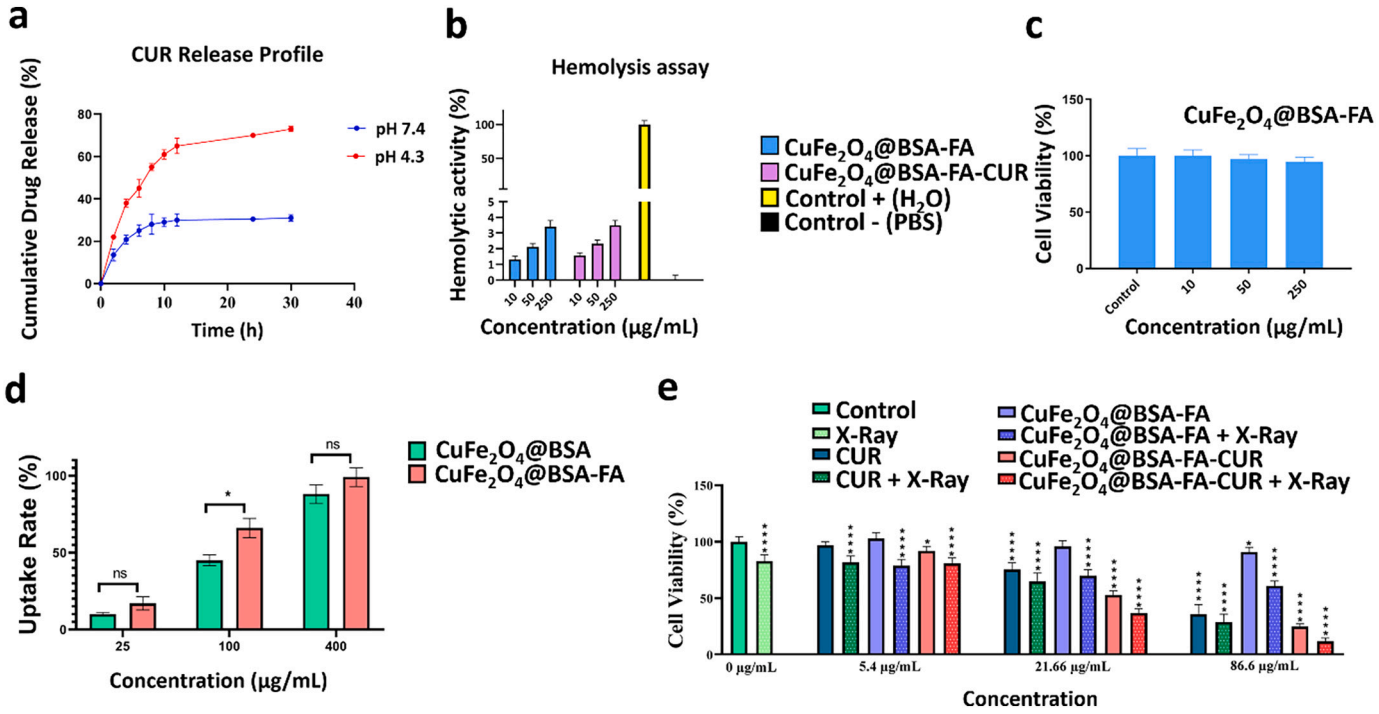

Fig. 4. *In vitro* drug release, biocompatibility and cytotoxicity assays. (a) Drug release profile, (b) Hemocompatibility of developed nanoradiosensitizers; (c) Cytotoxicity potential toward healthy cells; (d) Cell internalization and (c) *In vitro* radiosensitizing activity against 4T1 cells with or without X-ray irradiation.

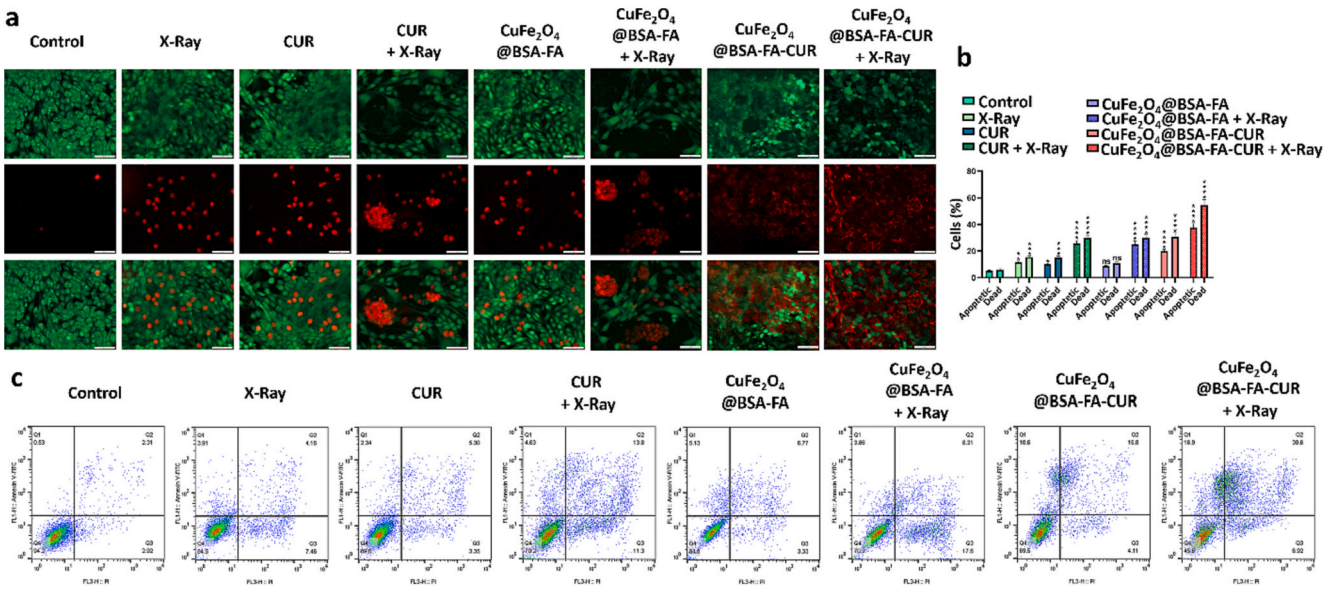

Fig. 5. *In vitro* antitumor activity of nanoradiosensitizer. (a) Fluorescence images of 4T1 cells after different treatments with calcein-AM/PI staining (scale bar = 50 μm); flow cytometry analysis: (b) Quantitative analysis of cell death and induction of apoptosis; (c) Potential of nanoradiosensitizer in induction of 4T1 cells apoptosis after exposing with different treatments and staining with annexin V-FITC/PI.

drug loading of CUR were found to be 83.82% and 21.66%, respectively. Also, to investigate whether the developed nanoradiosensitizers are sensitive to tumor microenvironment or not, drug release experiments were conducted under acidic (pH = 4.3) and normal physiological condition (pH = 7.4). The pH of tumor microenvironment is less than that of normal tissue, therefore developing a pH-responsive drug delivery systems is a very promising approach in favor of cancer treatment. This approach can also alleviate chemotherapy associated side effects, challenges and enhance drug accumulation within tumor tissues rather than normal tissues. Drug release profile of CUR from $CuFe_2O_4$@BSA-FA-CUR exhibited pH-dependent release behavior in a sustained/controlled way (Fig. 4a). In other words, release of CUR was accelerated under acidic pH compared to normal physiological environment. Depending on the dose, CUR can have a dual role, so that in high doses it has a radiation sensitizing role, and in low doses it has a radiation protection role. Accordingly, due to the pH-trigger release profile of CUR, it can be concluded that CUR in this case acts as a radiosensitizer in the acidic tumor environment. However, as shown in Fig. 4a, low amount of CUR is released under normal physiological pH, and as normal tissues have neutral pH, this can be protect to normal tissue as well. As a matter of fact, CUR acts as radiosensitizer agent within tumor tissue whereas it acts as a radioprotector agent for healthy tissues. In addition to these unique features, CUR has been reported to inhibit tumor growth and induce proapoptotic and antiproliferative effects through modulating several tumor growth factors and inhibition of signaling proteins [31,53]. Altogether, pH-dependent release behavior of CUR along with its multiple biological activities make the designed $CuFe_2O_4$@BSA-FA-CUR nanoradiosensitizer as a highly compelling tool for accomplishing efficient synergistic tumor radiotherapy.

4.4. *In vitro biosafety investigation*

4.4.1. *Analysis of hemocompatibility*

To achieve desired therapeutic effects, any chemotherapeutics such as developed $CuFe_2O_4$@BSA-FA nanoplatforms must first enter into the bloodstream to be carried toward the specific site of the action. In this case, they come into the direct contact with blood components, so their hemocompatibility is a major criterion and should not be overlooked. Besides, blood compatibility regards as a crucial assay in restricting the clinical applicability of blood-contacting nanomaterials. To clarify this, blood compatibility of $CuFe_2O_4$@BSA-FA and $CuFe_2O_4$@BSA-FA nanoplatforms was carried out. Both $CuFe_2O_4$@BSA-FA and $CuFe_2O_4$@BSA-FA-CUR nanoplatforms exhibited similar hemolysis rate of which the proportion of hemolysis increased as the concentration of tested samples increased (Fig. 4b). However, even at high concentration of these nanoplatforms, the degree of hemolysis remained very low (< 4%). These findings offer overwhelming indication for the safe clinical application of the developed $CuFe_2O_4$@BSA-FA-CUR nanoplatforms.

4.4.2. *Analysis of cytotoxicity against healthy cells*

Further tests should be carried out to strengthen our confidence in biosafety and biocompatibility of $CuFe_2O_4$@BSA-FA nanoplatforms to corroborate our initial findings in case of hemocompatibility. It has been well documented that MTT assay as a standard method of cell toxicity is generally utilized to clarify the cytotoxic potential of newly developed agents at the preclinical level. Hence, potential cytotoxicity of novel $CuFe_2O_4$@BSA-FA nanoplatforms against healthy cells should be studied prior to determining their *in vitro/vivo* radiosensitization capacities. The survival rate of HFF-2 cells after incubation with different concentrations of $CuFe_2O_4$@BSA-FA nanoparticles ranging from 10 to 250 μg/mL is shown in Fig. 4c. Interestingly, MTT findings discovered that $CuFe_2O_4$@BSA-FA nanoparticles exhibited no pernicious effects on cell survival rate not only at low concentrations but also at maximum tested dose. These results offer indisputable evidence for the biosafety of FA conjugated $CuFe_2O_4$@BSA for preclinical investigation.

4.5. *Cellular uptake and internalization efficacy*

The folate receptor (FR) seems to be a very promising target not only for cancer imaging but also cancer treatment, because it is overexpressed on a variety of cancer cells. Accordingly, in cancer cells, FA decorated nanoparticles are internalized *via* folate receptor-mediated endocytosis. Higher intracellular trafficking is thus anticipated for the FA decorated nanoparticles in comparison with nanoparticles without FA moieties. To clarify whether FA-conjugation is effective in cellular internalization or not, both $CuFe_2O_4$@BSA-FA and $CuFe_2O_4$@BSA nanoparticles were labeled with fluorescein isothiocyanate (FITC) and their efficacy in cellular internalization is assessed. This assay underlined the importance of FA as targeting moieties for efficient cellular uptake, since at concentration of 100 μg/mL there was a significant difference between

cellular internalization of FA conjugated $CuFe_2O_4$@BSA nanoparticles and non-FA-conjugated nanoparticles (Fig. 4d). As a matter of fact, intracellular trafficking and targeting capability of $CuFe_2O_4$@BSA nanoparticles are effectively enhanced by FA conjugation. FA conjugated nanoparticles increase the effectiveness of treatment through several ways such as an enhancement in their cellular uptake, restriction of their biodistribution and guiding them into the specific tumor site which diminish chemotherapy associated side effects as well. Based on the obtained data, $CuFe_2O_4$@BSA-FA nanoparticles showed higher cellular uptake compared to $CuFe_2O_4$@BSA nanoparticles. However, only $CuFe_2O_4$@BSA-FA nanoparticles at concentration of 100 μg/mL showed statistically higher cellular uptake compared to $CuFe_2O_4$@BSA nanoparticles. However, no significant difference was found between $CuFe_2O_4$@BSA and $CuFe_2O_4$@BSA-FA at concentration of 25 and 400 μg/mL. Hu et al. developed FA-conjugated gold nanostars for imaging and radiotherapy. The cellular internalization assay disclosed that FA-conjugated gold nanostars could potentially increase cellular uptake efficacy due to the presence of FA in the construction of final formulation which are consistent with our results [55]. It appears that in order to restrict the broad biodistribution of $CuFe_2O_4$@BSA nanoparticles and to improve their selective accumulation within the specific site or tissue, conjugation of targeting motifs are thus prerequisite.

4.6. In vitro anti-cancer activity

Given the excellent hemocompatibility, good biocompatibility and cell internalization enhancement of designed $CuFe_2O_4$@BSA-FA nanoplatforms, their radiosensitization effect was also assessed against the mouse breast carcinoma cell line (4 T1 cells) using MTT assay. Accordingly, in order to find out whether ROS-promoting nanomaterials such as developed $CuFe_2O_4$@BSA-FA-CUR nanoplatform is effective in killing cancer cells by enhancing the curative effect of radiation therapy or not, its therapeutic effects at three concentrations (5.40, 56.66 and 86.60 μg/mL of CUR and the equivalent amount carrier) were investigated. The radiosensitizing effects of CUR, $CuFe_2O_4$@BSA-FA and $CuFe_2O_4$@BSA-FA-CUR nanoparticles toward 4 T1 cells are shown Fig. 4e. It was found that X-ray radiation (4 Gy) can slightly inhibit the viability of 4 T1 cells in comparison with the control group. This emphasizes the importance of X-ray radiation (4 Gy) in radio oncology, but it did not declare that X-ray radiation alone is strong enough in controlling and suppressing the cancer cells. However, the role and usefulness of this technique in tumor shrinking is undeniable. No significant effect on the cell viability was observed once 4 T1 cells were treated with $CuFe_2O_4$@BSA-FA nanoparticles (5.40, 56.66 and 86.60 μg/mL). In contrary, once 4 T1 cells were treated with $CuFe_2O_4$@BSA-FA nanoparticles upon X-ray irradiation, strong cell radiosensitization was observed which resulted in significant decrease in cell viability rate. Moreover, with an increase in concentration of $CuFe_2O_4$@BSA-FA + X-ray, significant cytotoxicity was observed, which can be attributed to the cell radiosensitization effects of nanoparticles upon X-ray irradiation. Also, the potential cytotoxicity of CUR and in combination with X-ray were examined, and it was found that with increase in CUR concentration, significant cytotoxicity is observed. In addition, the combination of CUR with X-ray shows a greater therapeutic effect compared to CUR alone. Although, $CuFe_2O_4$@BSA-FA-CUR can decrease the survival rate of 4 T1 cells due to the presence of CUR in its structure, but the extraordinary anti-cancer activity was observed when the cells received co-treatment ($CuFe_2O_4$@BSA-FA-CUR + X-ray). This superior performance disclosed the advantages of combined therapy to monotherapy. The importance of synchronous chemoradiotherapy and radiation sensitizing capacity of the nanoparticles in radiation therapy is thus confirmed. The correlation between the concentration of nanoparticles and cell survival rate is striking, since by increasing the concentration, the cytotoxicity substantially increased as well. In other words, nanoradiosensitizers upon X-ray irradiation exhibited dose-dependent cytotoxicity. The lowest cell survival rate was observed when 4 T1 cells were irradiated in the presence of $CuFe_2O_4$@BSA-FA-CUR, which can be a good confirmation for synergistic anti-cancer and strong radiosensitizing effects. These results comply with Zhou et al.'s findings, where potent nanoradiosensitizers based on high Z element of Hafnium-based MOF (UiO-66-NH_2(Hf)) were developed which promoted cytotoxicity against cancer cell line of KYSE 150 by facilitating X-ray absorption *in vitro* [56]. Similar results were also reported by Wang and his colleagues [57]. Overall, it can be inferred that cancer cells are more vulnerable to X-ray accompanied by $CuFe_2O_4$@BSA-FA-CUR nanoplatforms demonstrating the usefulness of ROS-promoting nanomaterials in radiation-induced cancer therapy.

4.7. Calcein AM/PI cell staining assay

Calcein AM/PI cell staining assay, was employed to further assess the potential radiosensitizing effect of $CuFe_2O_4$@BSA-FA nanoparticles upon X-ray irradiation in induction of cell death. This assay provided simultaneous differentiation of dead and live cells in the tested specimen, of which PI and calcein/AM solutions stained dead and viable cells, respectively. As a result, Fig. 5a indicated the radiosensitizition activity of the CUR, $CuFe_2O_4$@BSA-FA and final developed $CuFe_2O_4$@BSA-FA-CUR in killing cells upon X-ray irradiation. There are green and red dots within a single fluorescence image of calcein AM/PI of which red dots represent the dead cells while green dots indicate the viable cells. As a matter of fact, presence of more green dots in the fluorescence image indicates a higher rate of cell survival (*e.g.*, control group), whereas the more the red dots mean a higher death rate ($CuFe_2O_4$@BSA-FA-CUR + X-ray group). Calcein AM/PI indicated that there are little red spots within the fluorescence image of the X-ray irradiation which reflects the inefficacy of this modality in induction of cell death. But, once 4T1 cells were irradiated by X-ray in the presence of developed nanoradiosensitizers, higher cell death was observed and the utility of $CuFe_2O_4$@BSA-FA-CUR nanoplatforms as an efficient radiosensitizer is thus underlined. As expected, strong radiosensitizing effect was observed for the $CuFe_2O_4$@BSA-FA-CUR + X-ray treatment group which led to the highest rate of cell death (Fig. 5a). This can be attributed to the use of Cu, Fe and CUR in the construction $CuFe_2O_4$@BSA-FA-CUR nanoparticles. Similar findings were reported by Gao et al., where they fabricated Bi_2S_3-MoS_2 nanoradiosensitizers for breast cancer theranostics. It was found that the proportion of dead cells increased once developed Bi_2S_3-MoS_2 nanoradiosensitizers were applied along with X-ray irradiation [58]. Taken together, these findings reveal that ROS-promoting nanomaterials such as $CuFe_2O_4$@BSA-FA-CUR is effective for killing cancer cells by enhancing the curative effect of radiation therapy.

4.8. Apoptosis assay

Flow cytometry technique was utilized to assess apoptotic potential $CuFe_2O_4$@BSA-FA-CUR. Following sample preparation, apoptotic potential of CUR, $CuFe_2O_4$@BSA-FA and $CuFe_2O_4$@BSA-FA-CUR were elucidated without and with simultaneous X-ray radiation (Fig. 5b,c). Cell population of early apoptosis, late apoptosis and non-apoptotic cell death phases differed in every group which is quantified and further presented in Fig. 5b. Potential of developed nanoparticles in cell death induction following X-ray irradiation was assessed. Cell death rate (apoptosis and non-apoptotic cell death) increased significantly in radiated cells when treated with CUR, $CuFe_2O_4$@BSA-FA and $CuFe_2O_4$@BSA-FA-CUR. $CuFe_2O_4$@BSA-FA-CUR effect in apoptosis/non-apoptotic cell death induction was most favorable when accompanied by X-ray radiation. Indeed, X-ray radiation could increase apoptotic and non-apoptotic cell death population in contrast to control group. The order of apoptosis induction and non-apoptotic cell death induction are as follows: Non-apoptosis cell death: $CuFe_2O_4$@BSA-FA-CUR + X-ray > $CuFe_2O_4$@BSA-FA-CUR > $CuFe_2O_4$@BSA-FA + X-ray > CUR + X-ray>CUR > X-ray > $CuFe_2O_4$@BSA-FA > Control.

Apoptosis: $CuFe_2O_4$@BSA-FA-CUR + X-ray > $CuFe_2O_4$@BSA-FA-CUR > $CuFe_2O_4$@BSA-FA + X-ray > CUR + X-ray > CUR > X-ray > Control.

Particularly, in radiotherapy cell exposure with CUR, $CuFe_2O_4$@BSA-FA and $CuFe_2O_4$@BSA-FA-CUR provided great benefits in cell death induction in contrast to radiotherapy alone, indicating the importance of Cu and Fe for sensitizing 4T1 cells to radiotherapy. In a closer look, CUR addition to $CuFe_2O_4$@BSA-FA nanoparticles had a good influence on cell apoptosis/non-apoptotic cell death and reached to the highest level when concurrently used with X-ray radiation. The findings support the statement that $CuFe_2O_4$@BSA-FA-CUR is a potent radiosensitizer for an efficient chemoradiotherapy in 4 T1 cells, highlighting the intrinsic properties of Fe and Cu in nanoparticle construction and synergistic therapeutic effect of CUR, which is entitled as a chemotherapeutic agent, upon addition to $CuFe_2O_4$@BSA-FA nanoparticles. The capability of $CuFe_2O_4$@BSA-FA-CUR nanoparticles to sensitization of 4T1 cells could originate from potentiation of ROS production and DNA damage upon X-ray exposure and probably FA involvement in intracellular trafficking and agent targeting capability. Similar results were also reported by Nosrati et al., where they fabricated Fe_3O_4–Au heterodimer decorated with FA as an effective radiosensitizer to enhance the radio-mediated cell death [54]. Our work has led us to conclude that the great cancerous cell death can be obtained by integration of chemoradiotherapy with nanoradiosensitizer, $CuFe_2O_4$@BSA-FA-CUR. Therefore, our satisfactory findings underline usefulness of devised nanoradiosensitizer as a powerful tool for induction of cell death.

4.9. *In vitro colony formation assay*

Following the *in vitro* results including calcein AM/PI cell staining assay, biocompatibility, apoptotic cell death and cellular uptake of developed nanosystems, *in vitro* colony formation assay, as a frequently used technique for evaluating reproductive of cancer cells death after irradiation [60], was performed to measure the radiosensitizing effect of nanoparticles. The clonogenic assay of cells treated with different treatment regimens after being exposed to the X-ray irradiation is represented in Fig. 6a,b. *In vitro* colony formation findings revealed that not only X-ray but also all of the treatment regimens can potentially inhibit cell reproduction. In other words, the analysis of colony formation showed that there were statistically significant differences between control group and other treatment groups in terms of survival fraction. The survival fraction of cells irradiated with X-ray in the presence of $CuFe_2O_4$@BSA-FA noticeably decreased compared to other groups which reflects the effective radiosensitization of developed nanosystems (Fig. 6b). To put it briefly, due to the strong radiosensitizing effect of $CuFe_2O_4$@BSA-FA-CUR upon X-ray irradiation, the colonies barely formed. It is important to note that these results have further strengthened our confidence in usefulness of Fe and Cu metals in construction of nanoradiosensitizers to generate highly reactive ROS products upon X-ray irradiation to confine the repopulation ability of malignant cells [61]. These appealing radiosensitizing effect of $CuFe_2O_4$@BSA-FA nanoparticles upon X-ray irradiation was not only repeated in clonogenic assay but also in the apoptosis assay, cellular uptake, *in vitro* anticancer assay and the live and dead cell staining (Calcein-AM/PI).

4.10. *Intracellular ROS generation*

ROS generation level inside 4T1 cells was assessed by utilizing DCFH-DA which oxidizes in ROS presence and emmitt green fluorescence as a result. Images of cell groups treated with nanoparticle and/or X-ray were sorted in Fig. 6c. Control and CUR group demonstrated no emitted light and thus no intracellular ROS production, while X-ray exposed cells indicated rare green fluorescence light which was comparable to emittance of radiation-exposed CUR-treated cells. Although no exposure occurred, fluorescent light intensity in cells treated with $CuFe_2O_4$@BSA-FA-CUR nanoparticles was slightly higher than that of X-ray and CUR + X-ray groups. Exposed cells with X-ray radiations provided higher amount of ROS in radiosensitizer presence ($CuFe_2O_4$@BSA-FA), and $CuFe_2O_4$@BSA-FA-CUR. By virtue of the fact that X-ray initiates ROS production, DNA damage occurs and cancerous cells die [62]. Considering higher fluorescence intensity observed in the case of nanoparticle treatment and concurrent radiation, elevated amount of ROS was produced in nanoparticle presence ($CuFe_2O_4$@BSA-FA and $CuFe_2O_4$@BSA-FA-CUR). This phenomenon unveils the importance of radioenhancers in radiotherapy in order to reach greater efficacy in ROS production and thus cell death compared to X-ray radiation alone. Induction of ROS level with cu based nanoparticles as a result of X-ray therapy with radioenhancers was also supported by previous investigations [63].

To sum up, the most striking result emerged from $CuFe_2O_4$@BSA-FA-CUR and X-ray simultaneous exploitation in cell radiotherapy which strengthen the statement that our fabricated nanomaterial can potentiate ROS generation upon X-ray exposure and thus is an effective radiosensitizer. Similar results were obtained in a recently-published study demonstrating radiosensitizing characteristic of nanoparticles composed of Fe and Cu [63]. *In vivo* and *in vitro* experiments proved that AuFCSP MOF could significantly enhance radiotherapy efficacy by implementation of high Z elements on an organic framework, produce hydroxyl radicals and enhance radiotherapy therapeutic efficacy [64]. Cell death fraction, apart from apoptosis, could be due to ferroptosis induced by iron. In fact, ferroptosis investigation was not a primary goal.

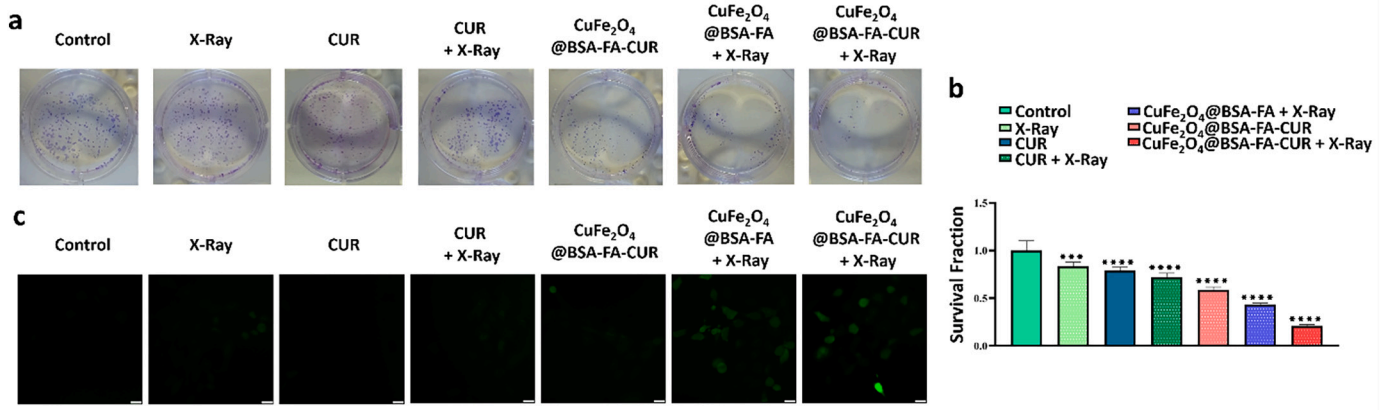

Fig. 6. *In vitro* antitumor activity of fabricated nanoradiosensitizer. (a) Representative photographs; and (b) Quantitative analysis of colony formation of cells irradiated by X-ray in the presence of different modalities (c) Potential capacity of developed $CuFe_2O_4$@BSA-FA-CUR nanoradiosensitizer in ROS production within 4T1 cells after treatment with DCFH-DA and being exposed to X-ray irradiation (Scale bar = 20 μm).

Nevertheless, we can still state that iron enhanced non-apoptotic cell death twice of X-ray radiation was used alone. This is in line with a recent study on Fe/Cu-containing MOF which could generate hydroxyl radicals mediated by Fenton/Fenton-like reaction [64]. It could be concluded that our nanostructure enhance intracellular ROS production and vanish radioresistance, a major obstacle in radiotherapy.

4.11. *In vivo* biosafety investigation

4.11.1. LD_{50} as an *in vivo* biosafety indicator

To confirm the *in vivo* biosafety of developed $CuFe_2O_4$@BSA-FA and accordingly increase the overall chances of these nanoplatforms to reach into the preclinical studies, *in vivo* biosafety was primarily assessed using LD_{50} assay. Mice received various concentrations of $CuFe_2O_4$@BSA-FA nanoparticles (50, 100, 200 and 400 mg/kg) by intravenous injection, and their survival rate and behavior were fully monitored. As depicted in Fig. S6, a Cox Regression diagram was used to represent the obtained results. Interestingly, after injection of $CuFe_2O_4$@BSA-FA, all mice survived and no deaths were observed in the treated groups, as well as monitoring of body weight reveled no significant changes relative to the control group. Furthermore, no significant side effects could be observed in the blood panel counts biochemical analysis after injection of $CuFe_2O_4$@BSA-FA-CUR (Fig. S7) [65]. These outcomes disclosed the fact that $CuFe_2O_4$@BSA-FA nanoparticles had no toxic effects and provided further evidence for *in vivo* biosafety of $CuFe_2O_4$@BSA-FA nanoplatforms for (pre)clinical exploration.

4.11.2. *In vivo* antitumor activity enhanced by X-ray irradiation

Various approaches have been put forward to fight against cancer, and among them radio oncology has long been accepted as an effective remedy in treatment of almost solid malignancies [66]. However, this conventional tool, due to the following shortcomings, is still far from being perfect: acute and/or late toxicity, damages to neighboring healthy tissues, radiotherapy by itself can not completely destroy tumors and risk of cancer recurrence remains as an overlooked challenge [67]. Additionally, emergence of radioresistance provoked researchers to design and fabricate integrated multifunctional nanoplatforms to solve the aforementioned issues and challenges. Recent advances in development of innovative radiosensitizers based on high-Z metals along with harnessing the power of nanotechnology have launched a novel treatment modality in cancer radiotherapy [68].

Before evaluation of *in vivo* therapeutic efficacy, the biodistribution of $CuFe_2O_4$@BSA and $CuFe_2O_4$@BSA-FA-CUR in xenografted 4T1 tumor and major organs were investigated by ICP-AES after typical tissue nitration. The result was shown in Fig. S8. Although the NPs accumulated in the reticuloendothelial system (RES) related organs, but NPs could still penetrate well in xenografted 4 T1 tumors. CuFe2O4@BSA-FA-CUR further improved nanoparticles accumulation in tumors. It was shown that $CuFe_2O_4$@BSA-FA-CUR has more tend to tumors rather $CuFe_2O_4$@BSA.

We evaluated the *in vivo* antitumor effects of $CuFe_2O_4$@BSA-FA and $CuFe_2O_4$@BSA-FA-CUR nanoparticles in the presence and absence of X-ray irradiation. This assay was initiated once tumors reached a mean volume of ~80 mm^3, then they were randomly divided into eight groups of five mice. *In vivo* mouse models of breast cancer were then treated with the following regimens: (1) CUR, (2) CUR with 4 Gy X-ray, (3) $CuFe_2O_4$@BSA-FA, (4) $CuFe_2O_4$@BSA-FA with 4 Gy X-ray, (5) $CuFe_2O_4$@BSA-FA-CUR, (6) $CuFe_2O_4$@BSA-FA-CUR with 4 Gy X-ray, (7) PBS and (8) X-ray. The *in vivo* tumor suppression effects of the foregoing groups following intravenous injection are shown in Fig. 7a. It is obvious that utilization of the conventional X-ray dose (4 Gy) by itself cannot meritoriously inhibit the tumor growth. Similar result was found by following intravenous injection of CUR, $CuFe_2O_4$@BSA-FA and $CuFe_2O_4$@BSA-FA-CUR nanoparticles, while astonishing results were observed once the treatments were combined with X-ray radiation (4 Gy). In the other words, co-use of X-ray radiation along with $CuFe_2O_4$@BSA-FA-CUR nanoparticles can potentially inhibit the tumor growth just by a single dose injection in comparison with other treatment plans. To put it briefly, the highest tumor growth inhibition was observed when the mice were treated with $CuFe_2O_4$@BSA-FA-CUR nanoparticles +4 Gy X-ray modality. This synergistic anticancer effect emphasizes the usefulness of $CuFe_2O_4$@BSA-FA-CUR as an effective potential radiosensitizer. The following order reflects the *in vivo* tumor suppression potential of combination therapy: $CuFe_2O_4$@BSA-FA-CUR with 4 Gy X-ray > $CuFe_2O_4$@BSA-FA with 4 Gy X-ray > $CuFe_2O_4$@BSA-FA-CUR > $CuFe_2O_4$@BSA-FA > CUR > X-ray. *In vivo* antitumor assay also highlighted that $CuFe_2O_4$@BSA-FA-CUR and $CuFe_2O_4$@BSA-FA nanoparticles without X-ray radiation, CUR with and without irradiation, X-ray radiation and PBS were not effective in the suppression of tumor growth. These findings may be attributed to the strong radiosensitization capacity of Cu and Fe elements which were utilized in the fabrication of $CuFe_2O_4$@BSA-FA. Moreover, accumulation of $CuFe_2O_4$@BSA-FA-CUR bimetallic nanoradiosensitizers within tumor sites is efficiently increased by FA moieties, and by X-ray irradiation, the degree of ROS level increased remarkably in the tumor tissue which is strongly favorable in cancer treatment. In fact, presence of FA moieties as targeting agent and CUR molecules as natural chemotherapeutic agent resulted in a strong synergistic inhibition of tumor growth. These findings appear to be well substantiated by Nosrati et al. findings of which remarkable *in vivo* tumor inhibition was observed by using a biocompatible folic acid (FA) decorated CUR-loaded Fe_3O_4–Au heterodimer (Fe_3O_4-Au-BSA-FA-CUR) nanoplatforms after X-ray irradiation [54]. Additionally, changes in body weight of mice in this assay within the experimental time periods were precisely measured (Fig. 7b). Surprisingly, no treatment groups showed any significant changes in body weight of mice. In fact, these results point out to the usefulness of $CuFe_2O_4$@BSA-FA-CUR nanoplatforms as a safe nanoradiosensitizer in enhanced synchronous chemoradiotherapy and synergetic tumor therapy.

4.12. *Histopathology analysis*

In order to reveal any possible toxicity of developed $CuFe_2O_4$@BSA-FA-CUR nanoparticles against mice major organs (kidney, spleen, liver and heart), histopathology analysis was conducted using hematoxylin & eosin (H&E) staining protocols. In this regard, on the 16th day of treatment, mice of different groups were euthanized, and their foregoing organs were collected to disclose whether fabricated nanoparticles in the presence of X-ray radiation can cause any toxicity or not. As shown in Fig. 7c, $CuFe_2O_4$@BSA-FA-CUR nanoplatforms had no obvious abnormalities on above mentioned organs compared to the control group. These results are also in line with that of observed for *in vitro/vivo* biosafety and biocompatibility results and prove the fact that $CuFe_2O_4$@BSA-FA-CUR nanoplatforms are practically nontoxic and their safety is thus validated. On the contrary, it is expected that $CuFe_2O_4$@BSA-FA-CUR nanoplatforms should cause damage to tumoral cells. Therefore, pathological H&E images of tumor tissue are also provided to ensure that the developed $CuFe_2O_4$@BSA-FA-CUR nanoplatform as a potent nanoradiosensitizer will fulfill its mission properly and effectively. Based on these results, it can be concluded that $CuFe_2O_4$@BSA-FA-CUR + X-ray could potentially damage tumor cells, as evidenced by the presence of more necrotic-shaped cells as well as extensive shadow area which complies with previous findings [54].

5. Conclusion

The projected nanoradiosensitizer aimed at gathering all pivotal influencing factors required for enhanced antitumor efficacy along with attenuating radiotherapy adverse effects in a single multifunctional newly synthesized nanoplatform called $CuFe_2O_4$@BSA-FA-CUR. Accordingly, in the current study, bimetallic nanoradiosensitizers based on Cu and Fe with enhanced intratumoral accumulation capability and

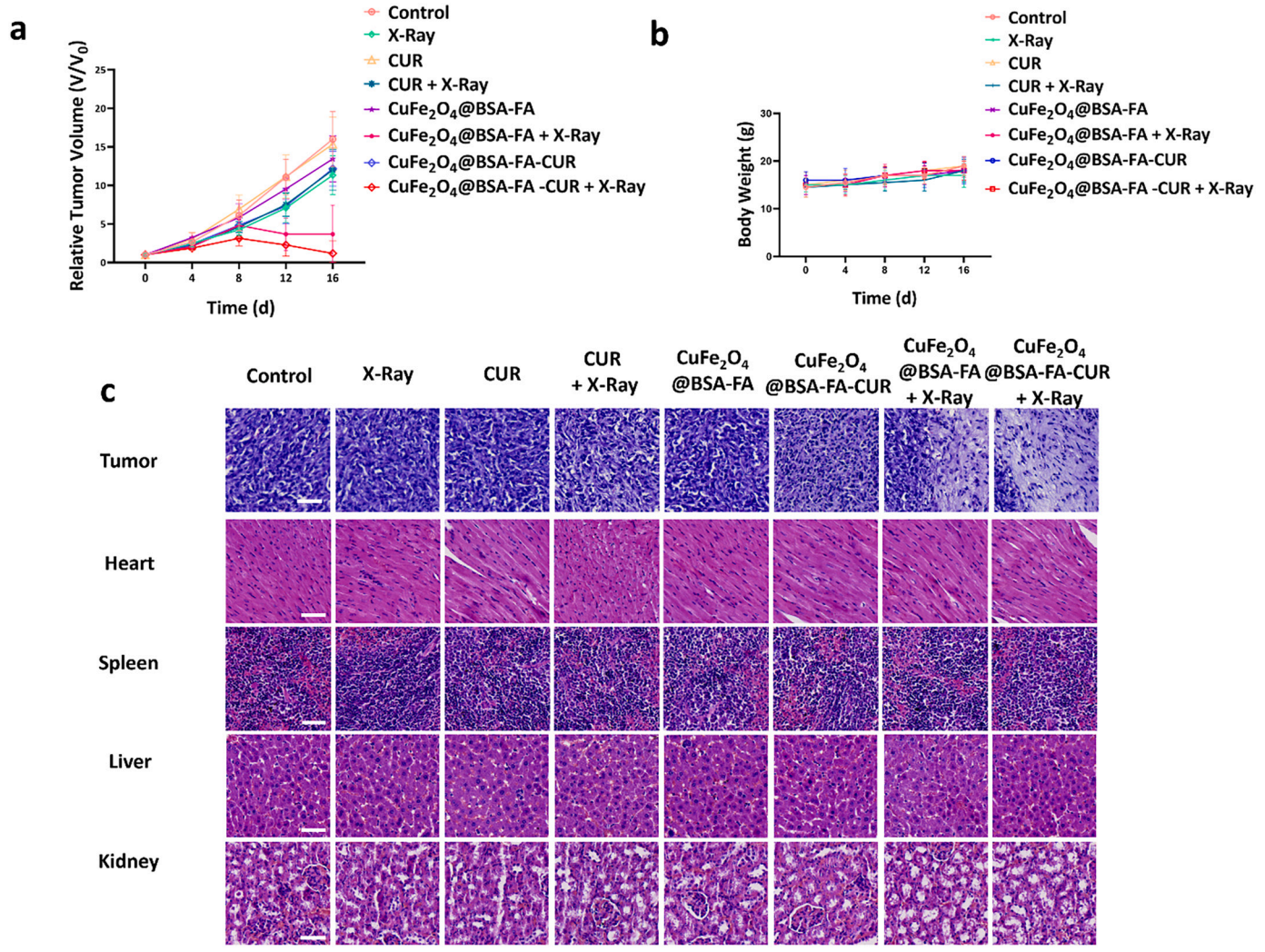

Fig. 7. *In vivo* studies of antitumor effects. (a) Relative tumor volumes following different treatments with or without X-ray irradiation; (b) Body weight of mice with different treatments; (c) Representative H&E staining of the tumor and main organs in the presence and absence of X-ray (scale bar = 50 μm).

desired physicochemical properties in terms of colloidal stability, favorable morphology and size were developed. *In vivo* and *in vitro* results confirmed that all aforementioned objectives were readily reachable by the utility of final nanoformulation. $CuFe_2O_4$@BSA-FA-CUR presented a great capacity in radiosensitization of tumor cells, whereas CUR displayed multifunctional roles on modulating radiation-induced cancer therapy through its intrinsic anti-tumor activity and radiosensitization effects. *In vitro* biological safety unveiled that $CuFe_2O_4$@BSA-FA-CUR nanoformulation did not cause any adverse effects. The most remarkable result to emerge from the data is that administration of $CuFe_2O_4$@BSA-FA-CUR nanoformulation + X-ray irradiation leads to complete ablation of tumors in a murine model. Altogether, this versatile nanoplatform offers new insights toward the application of multifunctional bimetallic nanoradiosensitizers for synchronous chemoradiotherapy with synergistic antitumor effects.

Ethical considerations

This study was approved by the Ethics Committee of the Iran National Science Foundation (Code: INSF-98018277), and the study participants signed an informed consent.

Data availability statement

The raw/processed data required to reproduce these findings cannot be shared at this time as the data also forms part of an ongoing study.

CRediT authorship contribution statement

Marziyeh Salehiabar: Conceptualization, Methodology, Software, Formal analysis, Investigation. **Mohammadreza Ghaffarlou:** Investigation, Software, Formal analysis. **Ali Mohammadi:** Investigation. **Navid Mousazadeh:** Investigation. **Hossein Rahimi:** Investigation. **Fatemeh Abhari:** Investigation. **Hamid Rashidzadeh:** Writing – original draft. **Leila Nasehi:** Resources, Investigation. **Hamed Rezaeejam:** Methodology, Investigation. **Murat Barsbay:** Formal analysis, Investigation, Writing – review & editing. **Yavuz Nuri Ertas:** Resources, Funding acquisition, Writing – review & editing. **Hamed Nosrati:** Conceptualization, Methodology, Software, Formal analysis, Investigation, Writing – review & editing. **Taras Kavetskyy:** Resources, Funding acquisition, Writing – review & editing. **Hossein Danafar:** Resources, Funding acquisition, Writing – review & editing.

Data availability

Data will be made available on request.

Acknowledgments

This work was supported by the "Iran National Science Foundation: INSF-98018277". We gratefully acknowledge the Zanjan University of Medical Science support. Y.N. Ertas acknowledges funding support from the 2232 International Fellowship for Outstanding Researchers Program of The Scientific and Technological Research Council of Türkiye (TÜBİTAK, Project No: 118C346). MB acknowledges the financial support of the International Atomic Energy Agency (IAEA) under coordinated research project F22070 (IAEA Research Contract No: 23192). T. K. acknowledges the financial support of the Ministry of Education and Science of Ukraine (projects Nos. 0121U109543 and 0122U000874), National Research Foundation of Ukraine (project No. 2020.02/0100 "Development of new nanozymes as catalytic elements for enzymatic kits and chemo/biosensors"), and SAIA (Slovak Academic Information Agency) in the framework of the National Scholarship Programme of the Slovak Republic.

References

[1] E. Hosseinzadeh, N. Banaee, Nedaie H. Ali, Cancer and treatment modalities, Cur. Cancer Ther. Rev. 13 (1) (2017) 17–27.
[2] D. Schaue, W.H. McBride, Opportunities and challenges of radiotherapy for treating cancer, Nat. Rev. Clin. Oncol. 12 (9) (2015) 527–540.
[3] D. De Ruysscher, G. Niedermann, N.G. Burnet, S. Siva, A.W. Lee, F. Hegi-Johnson, Radiotherapy toxicity, Nat. Rev. Dis. Primers 5 (1) (2019) 1–20.
[4] V. Vinnikov, M.P. Hande, R. Wilkins, A. Wojcik, E. Zubizarreta, O. Belyakov, Prediction of the acute or late radiation toxicity effects in radiotherapy patients using ex vivo induced Biodosimetric markers: a review, J. Personal. Med. 10 (4) (2020) 285.
[5] X. Lin, R. Zhu, Z. Hong, X. Zhang, S. Chen, J. Song, et al., GSH-responsive Radiosensitizers with deep penetration ability for multimodal imaging-guided synergistic radio-Chemodynamic Cancer therapy, Adv. Funct. Mater. 2101278 (2021).
[6] M. Babaei, M. Ganjalikhani, The Potential Effectiveness of Nanoparticles as Radio Sensitizers for Radiotherapy. BioImpacts: BI vol. 4(1):15, 2014.
[7] F. Zhang, S. Liu, N. Zhang, Y. Kuang, W. Li, S. Gai, et al., X-ray-triggered NO-released bi–SNO nanoparticles: all-in-one nano-radiosensitizer with photothermal/gas therapy for enhanced radiotherapy, Nanoscale. 12 (37) (2020) 19293–19307.
[8] Y.-W. Jiang, G. Gao, H.-R. Jia, X. Zhang, X. Cheng, H.-Y. Wang, et al., Palladium nanosheets as safe radiosensitizers for radiotherapy, Langmuir. 36 (39) (2020) 11637–11644.
[9] Y. Xie, Y. Han, X. Zhang, H. Ma, L. Li, R. Yu, et al., Application of new Radiosensitizer based on Nano-biotechnology in the treatment of glioma, Front. Oncol. 11 (2021) 855.
[10] L. Yu, X. Zhang, X. Li, Z. Zhang, X. Niu, X. Wang, et al., A pH-responsive Pt-based nanoradiosensitizer for enhanced radiotherapy via oxidative stress amplification, Nanoscale. 13 (32) (2021) 13735–13745.
[11] G. Tsakanova, A. Stepanyan, E. Arakelova, V. Ayvazyan, V. Tonoyan, A. Arakelyan, et al., The radioenhancement potential of Schiff base derived copper (II) compounds against lung carcinoma in vitro, PLoS One 16 (6) (2021), e0253553.
[12] Q. Huang, S. Zhang, H. Zhang, Y. Han, H. Liu, F. Ren, et al., Boosting the radiosensitizing and photothermal performance of Cu2–x Se nanocrystals for synergetic radiophotothermal therapy of orthotopic breast cancer, ACS Nano 13 (2) (2019) 1342–1353.
[13] M.M. Fathy, O.A. Saad, W.M. Elshemey, H.M. Fahmy, Dose-enhancement of MCF 7 cell line radiotherapy using silica-iron oxide nanocomposite, Biochem. Biophys. Res. Commun. 632 (2022) 100–106.
[14] F. Hadi, S. Tavakkol, S. Laurent, V. Pirhajati, S.R. Mahdavi, A. Neshastehriz, et al., Combinatorial effects of radiofrequency hyperthermia and radiotherapy in the presence of magneto-plasmonic nanoparticles on MCF-7 breast cancer cells, J. Cell. Physiol. 234 (11) (2019) 20028–20035.
[15] M. Mohammadian, S. Emamgholizadeh Minaei, Dezfuli A. Shiralizadeh, Improve the cytotoxic effects of megavoltage radiation treatment by Fe3O4@ Cus–PEG nanoparticles as a novel radiosensitizer in colorectal cancer cells, Cancer Nanotechnol. 13 (1) (2022) 1–21.
[16] W.M. Girma, S.-H. Tzing, P.-J. Tseng, C.-C. Huang, Y.-C. Ling, J.-Y. Chang, Synthesis of cisplatin (IV) prodrug-tethered CuFeS2 nanoparticles in tumor-targeted chemotherapy and photothermal therapy, ACS Appl. Mater. Interfaces 10 (5) (2018) 4590–4602.
[17] Z. Wang, Y. Wang, H. Guo, N. Yu, Q. Ren, Q. Jiang, et al., Synthesis of one-for-all type Cu5FeS4 nanocrystals with improved near infrared photothermal and Fenton effects for simultaneous imaging and therapy of tumor, J. Colloid Interface Sci. 592 (2021) 116–126.
[18] Q. Chen, Y. Luo, W. Du, Z. Liu, S. Zhang, J. Yang, et al., Clearable theranostic platform with a pH-independent chemodynamic therapy enhancement strategy for synergetic photothermal tumor therapy, ACS Appl. Mater. Interfaces 11 (20) (2019) 18133–18144.
[19] Y. Wang, L. An, J. Lin, Q. Tian, S. Yang, A hollow Cu9S8 theranostic nanoplatform based on a combination of increased active sites and photothermal performance in enhanced chemodynamic therapy, Chem. Eng. J. 385 (2020), 123925.
[20] R.K. Kankala, C.-G. Liu, A.-Z. Chen, S.-B. Wang, P.-Y. Xu, L.K. Mende, et al., Overcoming multidrug resistance through the synergistic effects of hierarchical pH-sensitive, ROS-generating Nanoreactors, ACS Biomat. Sci. Eng. 3 (10) (2017) 2431–2442.
[21] C.-G. Liu, Y.-H. Han, J.-T. Zhang, R.K. Kankala, S.-B. Wang, A.-Z. Chen, Rerouting engineered metal-dependent shapes of mesoporous silica nanocontainers to biodegradable Janus-type (sphero-ellipsoid) nanoreactors for chemodynamic therapy, Chem. Eng. J. 370 (2019) 1188–1199.
[22] Y. Yong, X. Cheng, T. Bao, M. Zu, L. Yan, W. Yin, et al., Tungsten sulfide quantum dots as multifunctional nanotheranostics for in vivo dual-modal image-guided photothermal/radiotherapy synergistic therapy, ACS Nano 9 (12) (2015) 12451–12463.
[23] K. Li, Y. Zhang, A. Hussain, Y. Weng, Y. Huang, Progress of photodynamic and RNAi combination therapy in Cancer treatment, ACS Biomat. Sci. Eng. 7 (9) (2021) 4420–4429.
[24] R.K. Kankala, P.-Y. Tsai, Y. Kuthati, P.-R. Wei, C.-L. Liu, C.-H. Lee, Overcoming multidrug resistance through co-delivery of ROS-generating nano-machinery in cancer therapeutics, J. Mater. Chem. B 5 (7) (2017) 1507–1517.
[25] D.M. Arvapalli, A.T. Sheardy, K. Allado, H. Chevva, Z. Yin, J. Wei, Design of curcumin loaded carbon nanodots delivery system: enhanced bioavailability, release kinetics, and anticancer activity, ACS Appl. Bio Mater. 3 (12) (2020) 8776–8785.
[26] M. Zhang, X. Zhang, T. Tian, Q. Zhang, Y. Wen, J. Zhu, et al., Anti-inflammatory activity of curcumin-loaded tetrahedral framework nucleic acids on acute gouty arthritis, Bioactive Mater. 8 (2022) 368–380.
[27] Q. Qiao, Y. Jiang, G. Li, Curcumin enhances the response of non-Hodgkin's lymphoma cells to ionizing radiation through further induction of cell cycle arrest at the G2/M phase and inhibition of mTOR phosphorylation, Oncol. Rep. 29 (1) (2013) 380–386.
[28] H. Nosrati, F. Abhari, J. Charmi, M. Rahmati, B. Johari, S. Azizi, et al., Facile green synthesis of bismuth sulfide radiosensitizer via biomineralization of albumin natural molecule for chemoradiation therapy aim, Artificial Cells Nanomed. Biotechnol. 47 (1) (2019) 3832–3838.
[29] N. Sebastia, A. Montoro, D. Hervas, G. Pantelias, V. Hatzi, J. Soriano, et al., Curcumin and trans-resveratrol exert cell cycle-dependent radioprotective or radiosensitizing effects as elucidated by the PCC and G2-assay, Mutat. Res. Fund. Mol. Mech. Mutagenesis 766 (2014) 49–55.
[30] B. Farhood, K. Mortezaee, N.H. Goradel, N. Khanlarkhani, E. Salehi, M.S. Nashtaei, et al., Curcumin as an anti-inflammatory agent: implications to radiotherapy and chemotherapy, J. Cell. Physiol. 234 (5) (2019) 5728–5740.
[31] K. Mansouri, S. Rasoulpoor, A. Daneshkhah, S. Abolfathi, N. Salari, M. Mohammadi, et al., Clinical effects of curcumin in enhancing cancer therapy: a systematic review, BMC Cancer 20 (1) (2020) 1–11.
[32] H. Rashidzadeh, S.J.T. Rezaei, S. Zamani, E. Sarijloo, A. Ramazani, pH-sensitive curcumin conjugated micelles for tumor triggered drug delivery, J. Biomater. Sci. Polym. Ed. 32 (3) (2021) 320–336.
[34] Z. Zou, H. Chang, H. Li, S. Wang, Induction of reactive oxygen species: an emerging approach for cancer therapy, Apoptosis. 22 (11) (2017) 1321–1335.
[35] H. Nosrati, M. Ghaffarlou, M. Salehiabar, N. Mousazadeh, F. Abhari, M. Barsbay, et al., Magnetite and bismuth sulfide Janus heterostructures as radiosensitizers for in vivo enhanced radiotherapy in breast cancer, Biomaterials Adv. 140 (2022), 213090.
[36] K. Wu, X. Chen, X. Chen, S. Zhang, Y. Xu, B. Xia, et al., Suberoylanilide hydroxamic acid enhances the radiosensitivity of lung cancer cells through acetylated wild-type and mutant p53-dependent modulation of mitochondrial apoptosis, J. Int. Med. Res. 49 (2) (2021) (0300060520981545).
[37] H. Nosrati, J. Charmi, F. Abhari, E. Attari, S. Bochani, B. Johari, et al., Improved synergic therapeutic effects of chemoradiation therapy with the aid of a co-drug-loaded nano-radiosensitizer under conventional-dose X-ray irradiation. *Biomaterials*, science 8 (15) (2020) 4275–4286.
[38] K. Morita, Y. Nishimura, S. Nakamura, Y. Arai, C. Numako, K. Sato, et al., Titanium oxide nano-radiosensitizers for hydrogen peroxide delivery into cancer cells, Colloids Surf. B: Biointerfaces 198 (2021), 111451.
[39] D. Li, M. Hua, K. Fang, R. Liang, BSA directed-synthesis of biocompatible Fe 3 O 4 nanoparticles for dual-modal T 1 and T 2 MR imaging in vivo, Anal. Methods 9 (21) (2017) 3099–3104.
[40] C. Zhang, Y.-Y. Fu, X. Zhang, C. Yu, Y. Zhao, S.-K. Sun, BSA-directed synthesis of CuS nanoparticles as a biocompatible photothermal agent for tumor ablation in vivo, Dalton Trans. 44 (29) (2015) 13112–13118.
[41] J. Zheng, Z. Lin, W. Liu, L. Wang, S. Zhao, H. Yang, et al., One-pot synthesis of CuFe 2 O 4 magnetic nanocrystal clusters for highly specific separation of histidine-rich proteins, J. Mater. Chem. B 2 (37) (2014) 6207–6214.
[42] G. Birlik Demirel, E. Aygul, A. Dag, S. Atasoy, Z. Cimen, B. Cetin, Folic acid-conjugated pH and redox-sensitive ellipsoidal hybrid magnetic nanoparticles for dual-triggered drug release, ACS Appl. Bio Mater. 3 (8) (2020) 4949–4961.
[43] P. Hu, X. Hou, X. Yu, X. Wei, Y. Li, D. Yang, et al., Folic acid-conjugated gold nanostars for computed tomography imaging and Photothermal/radiation combined therapy, ACS Appl. Bio Mater. 4 (6) (2021) 4862–4871.
[44] H. Tonbul, A. Sahin, E. Tavukcuoglu, G. Ultav, S. Akbas, Y. Aktas, et al., Folic acid decoration of mesoporous silica nanoparticles to increase cellular uptake and cytotoxic activity of doxorubicin in human breast cancer cells, J. Drug Deliv. Sci. Technol. 63 (2021), 102535.

[45] S. Chen, Y. Guo, J. Zhang, Y. Guo, X. Liang, CuFe2O4/activated carbon adsorbents enhance H2S adsorption and catalytic oxidation from humidified air at room temperature, Chem. Eng. J. 431 (2022), 134097.
[46] Y. Xu, J. Ai, H. Zhang, The mechanism of degradation of bisphenol a using the magnetically separable CuFe2O4/peroxymonosulfate heterogeneous oxidation process, J. Hazard. Mater. 309 (2016) 87–96.
[47] A. Carley, S. Jackson, J. O'shea, M. Roberts, The formation and characterisation of Ni3+—an X-ray photoelectron spectroscopic investigation of potassium-doped Ni (110)–O, Surf. Sci. 440 (3) (1999) (L868-L74).
[48] P. Mills, J. Sullivan, A study of the core level electrons in iron and its three oxides by means of X-ray photoelectron spectroscopy, J. Phys. D. Appl. Phys. 16 (5) (1983) 723.
[49] I. Nedkov, R. Vandenberghe, T. Marinova, P. Thailhades, T. Merodiiska, I. Avramova, Magnetic structure and collective Jahn–Teller distortions in nanostructured particles of CuFe2O4, Appl. Surf. Sci. 253 (5) (2006) 2589–2596.
[50] I. Nakai, Y. Sugitani, K. Nagashima, Y. Niwa, X-ray photoelectron spectroscopic study of copper minerals, J. Inorg. Nucl. Chem. 40 (5) (1978) 789–791.
[51] J. Epp, X-ray diffraction (XRD) techniques for materials characterization, in: Materials Characterization Using Nondestructive Evaluation (NDE) Methods, Elsevier, 2016, pp. 81–124.
[52] R. Kannaujia, V. Prasad, Rawat P. Sapna, V. Rawat, A. Thakur, et al., Facile synthesis of CuFe2O4 doped polyacrylic acid hydrogel nanocomposite and its application in dye degradation, Mater. Lett. 252 (2019) 198–201.
[53] C. Qi, D. Wang, X. Gong, Q. Zhou, X. Yue, C. Li, et al., Co-delivery of curcumin and capsaicin by dual-targeting liposomes for inhibition of aHSC-induced drug resistance and metastasis, ACS Appl. Mater. Interfaces 13 (14) (2021) 16019–16035.
[54] H. Nosrati, Y. Baghdadchi, R. Abbasi, M. Barsbay, M. Ghaffarlou, F. Abhari, et al., Iron oxide and gold bimetallic radiosensitizers for synchronous tumor chemoradiation therapy in 4T1 breast cancer murine model, J. Mater. Chem. B 9 (22) (2021) 4510–4522.
[55] P. Hu, X. Hou, X. Yu, X. Wei, Y. Li, D. Yang, et al., Folic acid-conjugated gold Nanostars for computed tomography imaging and Photothermal/radiation combined therapy, ACS Appl. Bio Mater. 4 (6) (2021) 4862–4871.
[56] W. Zhou, Z. Liu, N. Wang, X. Chen, X. Sun, Y. Cheng, Hafnium-based metal–organic framework nanoparticles as a radiosensitizer to improve radiotherapy efficacy in esophageal cancer, ACS Omega 7 (14) (2022) 12021–12029.
[57] X. Wang, C. Zhang, J. Du, X. Dong, S. Jian, L. Yan, et al., Enhanced generation of non-oxygen dependent free radicals by schottky-type heterostructures of au–Bi2S3 nanoparticles via X-ray-induced catalytic reaction for radiosensitization, ACS Nano 13 (5) (2019) 5947–5958.
[58] F. Gao, D. Wang, T. Zhang, A. Ghosal, Z. Guo, Y. Miao, et al., Facile synthesis of Bi2S3-MoS2 heterogeneous nanoagent as dual functional radiosensitizer for triple negative breast cancer theranostics, Chem. Eng. J. 395 (2020), 125032.
[60] J. Xiao, L. Zeng, S. Ding, Y. Chen, X. Zhang, Bian Xw, et al., Tumor-tropic adipose-derived mesenchymal stromal cells mediated Bi2Se3 nanoradiosensitizers delivery for targeted radiotherapy of non-small cell lung cancer, Adv. Healthc. Mater. (2022) 2200143.
[61] X. Dong, R. Cheng, S. Zhu, H. Liu, R. Zhou, C. Zhang, et al., A heterojunction structured WO2. 9-WSe2 nanoradiosensitizer increases local tumor ablation and checkpoint blockade immunotherapy upon low radiation dose, ACS Nano 14 (5) (2020) 5400–5416.
[62] K. Ni, G. Lan, W. Lin, Nanoscale metal–organic frameworks generate reactive oxygen species for cancer therapy, ACS Central Sci. 6 (6) (2020) 861–868.
[63] Y. W. Jiang, G.Gao, H. R. Jia, X. Zhang, J. Zhao, N. Ma, et al. Copper oxide nanoparticles induce enhanced radiosensitizing effect via destructive autophagy. *ACS Biomaterials Science & Engineering*, *5*(3), (2019).1569-1579.
[64] Y. Liang, C. Peng, N. Su, Q. Li, S. Chen, D. Wu, et al., Tumor microenvironments self-activated cascade catalytic nanoscale metal organic frameworks as ferroptosis inducer for radiosensitization, Chem. Eng. J. 437 (2022), 135309.
[65] J. Zhou, W. Zhao, Z. Miao, J. Wang, Y. Ma, H. Wu, et al., Folin–ciocalteu assay inspired polyoxometalate nanoclusters as a renal clearable agent for non-inflammatory photothermal cancer therapy, ACS Nano 14 (2) (2020) 2126–2136.
[66] D. Luo, A. Johnson, X. Wang, H. Li, B.O. Erokwu, S. Springer, et al., Targeted radiosensitizers for MR-guided radiation therapy of prostate cancer, Nano Lett. 20 (10) (2020) 7159–7167.
[67] M. Loi, T. Comito, C. Franzese, L. Dominici, L.L. Faro, E. Clerici, et al., Stereotactic body radiotherapy in hepatocellular carcinoma: patient selection and predictors of outcome and toxicity, J. Cancer Res. Clin. Oncol. 147 (3) (2021) 927–936.
[68] L. Zeng, Y. Cao, L. He, S. Ding, X.-w. Bian, G. Tian, Metal–ligand coordination nanomaterials for radiotherapy: emerging synergistic cancer therapy, J. Mater. Chem. B 9 (2) (2021) 208–227.